Journal of Hydrology 640 (2024) 131700

Contents lists available at ScienceDirect

Journal of Hydrology

journal homepage: www.elsevier.com/locate/jhydrol

Research papers

DFEAT: A multifaceted yearly Drought FEature Assessment Tool from daily soil water content

Georgie Elias [a], Ghaleb Faour [b], Florent Mouillot [a,*]

[a] Centre d'Ecologie Fonctionnelle et Evolutive CEFE, UMR 5175, CNRS, Université de Montpellier, EPHE, IRD, 1919 Route de Mende, CEDEX 5, 34293 Montpellier, France

[b] National Center for Remote Sensing, National Council for Scientific Research (CNRS), Riad al Soloh, Beirut 1107 2260, Lebanon

ARTICLE INFO

This manuscript was handled by Andras Bardossy, Editor-in-Chief, with the assistance of Szilágyi József, Associate Editor

Keywords:
Automated tool
Drought Feature
Multifaceted Drought
KBDI
Soil Water content

ABSTRACT

The characterization of yearly drought events represents a key information for conducting impact assessments and forecasting future threats, and usually relies on a single index of duration or severity. Mostly based on daily soil or atmospheric water balances, the derivation of key drought facets is not yet standardized or embedded in a single tool, thus limiting intercomparisons between studies. We developed DFEAT as a fully-automated tool designed to characterize yearly drought features, based on any simulated/observed/remotely sensed soil water content time series. We provide here an application assessment performed with the Keetch-Byram Drought Index (KBDI) as a standard daily soil water model over a 60-year period and covering the Mediterranean aridity gradient in Lebanon (Middle-East) experiencing humid to semi-arid climate conditions. We computed and tested 19 drought features related to duration, severity, onset, offset, drying and wetting rates, driest peak day, and rainfall pulses across three soil water desiccation thresholds. For our study area, we revealed the uncorrelated specificities of 6 features, allowing to regionally discriminate between mountainous Mediterranean climate experiencing shorter drought duration (45 days), later onset (Day of the Year = 198), less rainfall pulses intensities (3.35 mm), and slower drying (1.68 mm/day) and wetting (−2.72 mm/day) rates, but similar offset date (Day of the Year = 356) compared to the coast. DFEAT also captured regions with prolonged Multi-Year Droughts not fully refilling field capacity under arid bioclimate reaching up to 22 years. We demonstrate here the applicability of DFEAT across water-limited bioclimates and the non-correlation between drought features with contrasted agro-ecological impacts.

1. Introduction

Drought, as a natural climatic phenomenon, occurs in every hydroclimatic region. It can be defined as a climatic condition experiencing a prolonged shortage in water supply resulting from insufficient precipitations, particularly prevalent in arid or semi-arid regions where the rainfall pattern exhibits high variability (Glantz, 2003). Drought can recur as a phenomenon, becoming a major concern when it reaches a threshold that stresses a number of agricultural, ecological, hydrological, and biophysical processes with socio-economic implications (Wilhite and Glantz, 1985). The complexity of drought is heightened by a sequence of processes that unfolds in a cascading manner, leading to challenges to the scientific community in uniformly quantifying drought across disciplines (Tramblay et al., 2020).

In order to quantify these drought phenomena, and investigate their interannual and regional variability as well as the impacts of climate change, a set of precipitation-based indices have been proposed for IPCC reports (Gutiérrez et al., 2021; Han and Singh, 2023; Lee et al., 2023; Pachauri et al., 2014) and implemented in the Rclimdex tools (Shrestha et al., 2017; Zhang and Yang, 2004). They mostly refer to yearly information on precipitation amounts, dry spells, and occurrences of extreme precipitation events (Meteorological indices). In a more integrative way, the Standardized Precipitation Index (SPI), a widely used drought index relying solely on precipitation data, has emerged as a main tool in operational drought monitoring. Introduced by McKee et al (1993) and further elaborated by Edwards and McKee (1997), the SPI assesses monthly precipitation anomalies at a specific location by comparing observed total precipitation levels over a defined accumulation period (e.g., 1, 3, 12, or 48 months) with the long-term historical rainfall data for that corresponding period. More recently, Vicente-Serrano et al

* Corresponding author.
E-mail address: florent.mouillot@ird.fr (F. Mouillot).

https://doi.org/10.1016/j.jhydrol.2024.131700
Received 10 April 2024; Received in revised form 26 June 2024; Accepted 8 July 2024
Available online 20 July 2024

(2010) combined Potential Evapotranspiration (PET) and SPI into the Standardized Precipitation Evapotranspiration Index (SPEI). Beside the direct use of these indices for agro-ecological assessments (Gao et al., 2018; Vicente-Serrano et al., 2012; Vicente-Serrano et al., 2014), recent studies could derive additional features such as drought onset, offset, peak drought month, and intensification rate as key drivers of agro-ecosystems functioning (Beyene et al., 2023; Fung et al., 2020; Iglesias et al., 2022; Mathbout et al., 2021; Rahmat et al., 2015; Wang et al., 2021; Yoo et al., 2022). We could, however, deplore an intrinsic lack of temporal precision on a monthly time resolution. Nevertheless, these recent studies highlight the multifaceted nature of drought events and their intricated implications (Beyene et al., 2023; Gao et al., 2018), so that a single drought index appears insufficient to cover all drought impact assessments (Zargar et al., 2011).

Daily soil water balance models, simulating a temporal information on soil water content (mm/day), could provide a more detailed and dynamic picture of drought compared to monthly or seasonal indices, including rainfall pulses or deep drainage during extreme events when rainfall inputs exceed the capacity of soil to retain this water (Deo et al., 2017; Lu et al., 2014).

Empirical soil water budget models as, among others, the Keetch-Byram Drought Index (Keetch and Byram, 1968), are tailored to reflect the impact of daily meteorological anomalies on soil water loss (further called water depletion measured in mm/day), relying on precipitation data and accounting for water that integrates soil layers (i.e., upper and duff soil layers). Based on this daily soil water content (or desiccation to field capacity defining the daily drought intensity), already standard yearly integration of drought features can be implemented more precisely as severity, duration, and timing (onset and offset), more readily usable than the raw meteorological measures used for their calculation (Zargar et al., 2011). Drought onset can be defined by the day when soil water content falls below a threshold, while drought offsets is determined when a large amount of rainfall increment to the hydrological cycle will replenish soil moisture above that threshold, with drought duration and severity directly derived from these timings (Liu et al., 2021; Tsakiris et al., 2007; Yoo et al., 2022; Zargar et al., 2011).

Heretofore, a comprehensive understanding of a drought event and its associated impacts on agriculture and ecosystems, entails multiple facets of the soil water content dynamic across the dry period, surpassing the confines of a singular drought feature (Beyene et al., 2023; Gao et al., 2018). Yet, to date, this domain is comparatively underexplored, presenting an ongoing frontier for exploration and there are currently only few attempts having targeted the characterization of yearly drought features through a daily measured or simulated water balance (Deo et al., 2017; Hunt et al., 2009; Kim et al., 2011; Lu, 2009; Lu et al., 2014; Ruffault et al., 2013; Zhang et al., 2022; Zribi et al., 2016), yet no consensus on a generic tool to generate these features has been proposed.

Accordingly, this study aims at presenting DFEAT, an automated tool for drought features identification, designed to discern and extract a set of yearly drought features derived from a daily soil water desiccation time series. We have tested this tool with the Keetch-Byram drought index over Lebanon, a Mediterranean drought-prone region covering a climate gradient from Mediterranean sub-humid to arid and present here its application, genericity, and sensitivity to climate uncertainty.

2. Materials and methods

2.1. Study area

Lebanon is located on the eastern coast of the Mediterranean Sea (Fig. 1a), covering an area of 10,452 km^2 between 33°–35°N and 35°–37°E (Shaban, 2020). Lebanon hosts a harsh topography providing

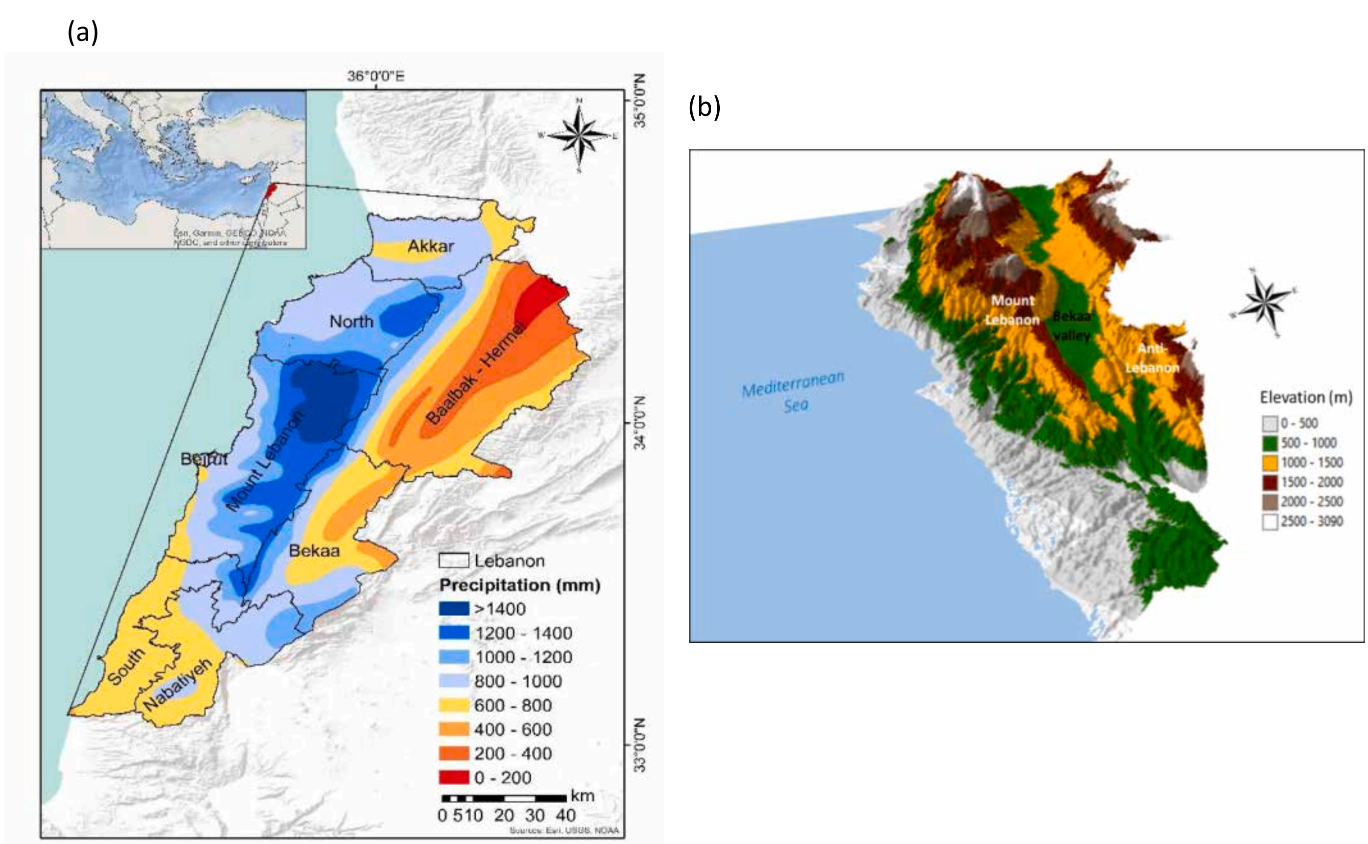

Fig. 1. a) Rainfall map of Lebanon (modified from Plassard, 1971), b) the major geomorphological slope units of Lebanon (Mount-Lebanon, Bekaa Valley, and Anti-Lebanon).

various microclimates from Mediterranean to arid, representative of the whole Mediterranean basin. Three major geomorphological features exist (Fig. 1b). The Anti-Lebanon mountain chain runs North/South parallel to the Mount-Lebanon chain and the Mediterranean coast, separated by the agricultural Bekaa Plain. The two parallel mountain ridges of Lebanon, which overlook the Mediterranean Sea, serve as a meteorological barrier. This barrier intercepts the cold air masses originating from the Mediterranean sea and causes them to condense into rain and snow (Shaban et al., 2019). Accordingly, this topographic complexity of mountainous regions across the country results in a high spatial variability in precipitation (Jomaa et al., 2019), with high annual rainfall amounts occurring on the high mountainous regions (>1200 mm) and predominant semi-humid to humid climate in the coastal zone (around 800 mm) (Fig. 1a). Arid-climate is located in the Northeastern part of Lebanon (Shaban et al., 2019) with annual rainfall amounts being lower than 600 mm. Under a typical Mediterranean climate with four distinct seasons, warm and dry summer and wet winter, the rainfall pattern follows a seasonal distribution, primarily occurring between the months of October and March (Kobrossi et al., 2021). The four consecutive months, June to September, constitute the warmest period of the year and experience relatively low levels of precipitation. The average winter temperature is 13 °C on the coast, decreasing with altitude. In summer, the average temperature is 29 °C (Shaban, 2020).

2.2. Meteorological data

We used the daily ERA5-Land dataset over the period 1960–2020. ERA5-Land is an open-source climatic dataset with a global spatial resolution of 9 km, simulated hourly by global high-resolution numerical integrations of the ECMWF land surface model driven by the downscaled meteorological forcing from the ERA5 climate reanalysis, including an elevation correction for the thermodynamic near-surface state (Muñoz-Sabater et al., 2021). ERA5-Land data, offering the finest resolution with the open-source climate data, have been widely used in climate impact research and have been locally acknowledged for their good performance (Gatien et al., 2023; Gomis-Cebolla et al., 2023). For our study, the climatic variables downloaded all over Lebanon were air temperature (K) at 2 m and total precipitation (m) for the selected time period. However, ERA5-Land data are unavailable for certain pixels near the coastal zones, as ERA5-Land relies on a network of observations and satellite data, and in some instances, these sources may not provide adequate coverage or resolution near coastlines.

2.3. Keetch-Byram drought index (KBDI)

The Keetch-Byram drought index (KBDI, Keetch and Byram, 1968) is an indicator of soil water deficit to field capacity (i.e., maximum amount of water that a soil can hold after draining and measured in mm) based on a simplified water-balance model simulating daily soil water loss per day. The index is widely used in wildfire monitoring (Ainuddin and Ampun, 2008; Brown et al., 2021; Liu et al., 2010; Varol and Ertuğrul, 2016) through the flammability of organic materials within the ground (Novitasari et al., 2019), fire management (Dimitrakopoulos and Bemmerzouk, 2003; Ganatsas et al., 2011), and fire hazard prediction (Hamadeh et al., 2015; Nogueira et al., 2017; Zhao and Liu, 2021). In addition, it was used in climate change (Gannon and Steinberg, 2021) and agricultural research studies (Salehnia et al., 2018). The index calculation requires few meteorological data: daily maximum temperature (Tmax), daily precipitation (P), and the mean annual precipitation data (Py). It is a cumulative index of the litter and duff layer desiccation, calculated as a balance between soil water input from effective precipitation (Eq. (1)) and an empirical model that approximates the actual evapotranspiration from daily soil desiccation (Eq. (2)) and temperature-based evaporative demand (i.e., PET) (Liu et al., 2010) (Eqs. (3), (4)). We define here soil desiccation as the soil water deficit to field capacity and soil water depletion as the daily soil water loss based on Zhang et al (2023). Note that in KBDI initial document (Keetch and Byram, 1968), you will find soil depletion defined as our soil desiccation, a concept that was not fully standardized at the time.

The KBDI initial version assumes that the field capacity of the upper soil/duff layer is 8 in. (203 mm), a strong assumption as this field capacity is not always true, since it depends on soil texture and depth, but kind of a fair value within the superficial rocky soils observed in Mediterranean ecosystems (Ganatsas et al., 2011; Häusler et al., 2019; Pellizzaro et al., 2007; Ruffault et al., 2013; Zribi et al., 2016). In Equation (3), soil moisture is assumed to saturate at 8 in. and the KBDI values are then constrained to a maximum value of 800 (unit: 0.01 in.).

The corresponding formulas are:

$$P_{net} = \max(0, P_t - 0.2) \tag{1}$$

$$Q_t = (KBDI_{t-1}) - P_{net} \tag{2}$$

$$dQ = \frac{10^{-3}(800 - Q_t)(0.968e^{0.0486T} - 8.3)dt}{1 + 10.88e^{-0.0441R}} \tag{3}$$

$$KBDI_t = Q_t + dQ \tag{4}$$

Where $KBDI_t$ and $KBDI_{t-1}$ are the KBDI values of the current (t) and previous (t-1) days, respectively. dQ is the drought factor, which reflects the daily change in dryness index, where T is the daily maximum temperature (in F°) at 2 m above the ground, P is the daily precipitation (inches), R is the mean annual rainfall (inches), and dt is a time increment set equal to one day. On each day, a value for the soil water depletion (Q_t in 0.01 in.) is computed as the KBDI from the previous day ($KBDI_{t-1}$) minus the net rainfall (P_{net} in inches) of the current day (Eq. (2)). In order to obtain P_{net}, 0.2 in. (5 mm) has to be subtracted from any daily rainfall amount exceeding 0.2 in. (Eq. (1)). If the daily rainfall amount is smaller than 0.2, then net rainfall equals zero (Snyder et al., 2006).

This initial equation was then further converted by Crane (1982), to international units with temperature in degrees Celsius (°C) and rainfall in millimeters (mm). The daily change in drought factor (dQ), measured in mm, is then expressed as shown in Eq. (5):

$$dQ = \frac{10^{-3}(203.2 - Q_t)(0.968e^{0.0875T+1.5552} - 8.3)dt}{1 + 10.88e^{-0.001736R}} \tag{5}$$

A modified version of the index (Eq. (6)) was proposed by Ganatsas et al (2011), by adapting the variables of Tmax and the mean annual rainfall (Py) to adjust KBDI to Mediterranean conditions. This entails adjusting $KBDI_t$ calculations to also account for a reduction from 5 mm to 3 mm when computing net rainfall (P_{net}).

$$dQ = \frac{10^{-3}(200 - Q_t)(1.713e^{0.0875T+1.5552} - 14.59)\,dt}{1 + 10.88e^{-0.001736R}} \tag{6}$$

The KBDI index has been used in Lebanon for investigating the drought-related seasonality of fire hazard (Hamadeh et al., 2017; Karouni et al., 2013; Mitri et al., 2014a, 2014b). Furthermore, it has been tested in several Mediterranean countries to assess its effectiveness in reproducing the live fuel moisture seasonal dynamics of various Mediterranean shrubs species (Pellizzaro et al., 2007; Ruffault et al., 2018). We have then hypothesized that such a daily drought index is enough adequate to fairly represent daily soil Available Water Content (AWC) for testing our drought assessment tool over the Mediterranean climates of Lebanon. Accordingly, in our study, we have employed the Mediterranean-adapted version of the KBDI index (Eq. (6)).

2.4. Characterization of annual drought features from daily KBDI time series

2.4.1. Fine fitting of wetting and drying curves

We aim here at characterizing each hydrological year into key features based on the daily KBDI. Most studies have utilized a standard 12-month calendar year (365 days), overlooking that drought may extend beyond December 31st. In Lebanon, hydrological years do not strictly adhere to the conventional calendar days (i.e., DOY); instead, we defined the hydrological year as the period starting on the 1st January, and finishes on the day when the soil is replenished to its field capacity of 203 mm (KBDI=0) after a seasonal drought. Between these starting and ending points representing the hydrological year, we fitted a smoothed time course of daily KBDI based on 'Phenofit' (Kong et al., 2022), a statistical framework previously developed for characterizing plant phenological phases based on the remotely sensed time series of leaf area. The rationale for utilizing this framework hinges on its inclusion of various curve-fitting methods, with an increasing phase and a decreasing phase representative of the soil desiccation curve observed under Mediterranean climate conditions. Currently, five fine curve fitting methods are provided in 'Phenofit' to reconstruct daily time series, namely 'Elmore' (Elmore et al., 2012), 'Zang' (Zhang et al., 2003), 'Gu' (Gu et al., 2009), 'Beck' (Beck et al., 2006), and 'AG' (Jönsson and Eklundh, 2004). Their equations differ in the number of parameters, thereby varying their levels of flexibility. Kong et al (2020) assessed their performance and suggested that the logistic nature of the Elmore and Beck equations outperforms the other equations, significantly influencing the accuracy of metrics extracted from the reconstructed time series. We have compared both methods and found that, in general, they yield similar results in the measured R-squared (goodness of fit). However, in some cases of abrupt changes in the KBDI time series, the Elmore-fitted curve tends to exhibit greater flexibility. Accordingly, we have retained the Elmore dual logistic Fine Curve Fitting equation (Elmore et al., 2012) (Fig. 2a). This dual logistic formula contains a positive, increasing curve (drying curve), which will represent drought onset and intensification rates (onset and development stages) until reaching a maximum value (persistence/peak KBDI stages), and includes a non-flat "greendown" maximum plateau (Fig. 2b), allowing for more flexibility than the Beck equation. On the other hand, the negative decreasing curve (wetting curve), represents the soil moisture replenishment (recovery and offset stages) after rainfall pulses events, presented as short-term increase in soil moisture content due to episodic rains (Bonsal et al., 2011; Brown et al., 2022; Collins et al., 2014), and dynamics precipitation increments of the early rainy season (Ferijal et al., 2022). Using these fitted curves enables the determination of a singular value for drought onset and offset day of the year, thus avoiding potential rainfall pulses impacts generating multiple crossings of the KBDI curve with the soil desiccation thresholds. It also allows for an objective calculation of drying and wetting rates smoothed over the time series with potential rainfall pulses during the drying or wetting phases.

2.4.2. Drought features characterization

We decided to set three KBDI thresholds: low (KBDI-50), moderate (KBDI-100), and extreme (KBDI-150), corresponding respectively to soil desiccation reaching 25 %, 50 %, and 75 % of AWC, following thresholds of Andrade and Bugalho (2023). We defined drought onsets for each KBDI threshold as the unique Day-Of-the-Year (DOY) when these thresholds are met in the drying curve and we defined offsets as the unique DOY when the thresholds are met in the wetting curve. We'll note here that onset DOY is always above 1, assuming that drought starts after January 1st as defined in our hydrological year, but see section 2.4.3 for Multi-Year Droughts characterization. Offset DOY can reach values above 366 when drought is prolonged after December 31st of the current year.

Once we have defined the three-drought onset and offset DOY, the duration and severity of each event could be derived. Drought duration was calculated as the number of consecutive days between the offset and onset DOY. Drought Intensity (DI), Severity (DS), or Magnitude (DM) are three terms that could potentially hold similar definitions but may vary in the existing literature on drought (Espinosa et al., 2019; Mathbout et al., 2021; Oukaddour et al., 2024; Zargar et al., 2011). Here we define the term drought severity (DS) as the sum of KBDI values between the onset and offset DOY of each soil desiccation level. This approach is consistent with previous drought severity estimates following a threshold level method (Deo et al., 2017; Kim et al., 2011; Mathbout et al., 2021; Ruffault et al., 2013; Yevjevich, 1967). When KBDI doesn't reach a KBDI threshold, onset and offset are set to 'NA' and DD and DS are set to 0.

We then defined the peak KBDI (Peak.KBDI) of the hydrological year corresponding to the maximum KBDI values, and its timing (Peak.KBDI.DOY) when this peak is reached (Deo et al., 2017). After pinpointing Peak.KBDI.DOY, we calculated the total count (RP.Num) of episodic rainfall pulses between this Peak.KBDI.DOY and the day of extreme drought offset (Extreme.D.Offset). These pulses are defined as a narrow window of low water inputs, following an extended period of water stress (López-Ballesteros et al., 2016). Rainfall pulses (RP) are automatically identified when the actual KBDI value on the following day is lower (wetter) than the current day (Rainfall pulse start RPS). The end of a rainfall pulse (RPE) is marked when two consecutive days have similar index values or when the KBDI value on the next day exceeds that of the previous day. Subsequently, we calculated each rainfall pulse intensity as the sum of the daily KBDI decrease starting from RPS+1 to RPE, and we finally calculated their mean (RP.I.mean) and standard deviation

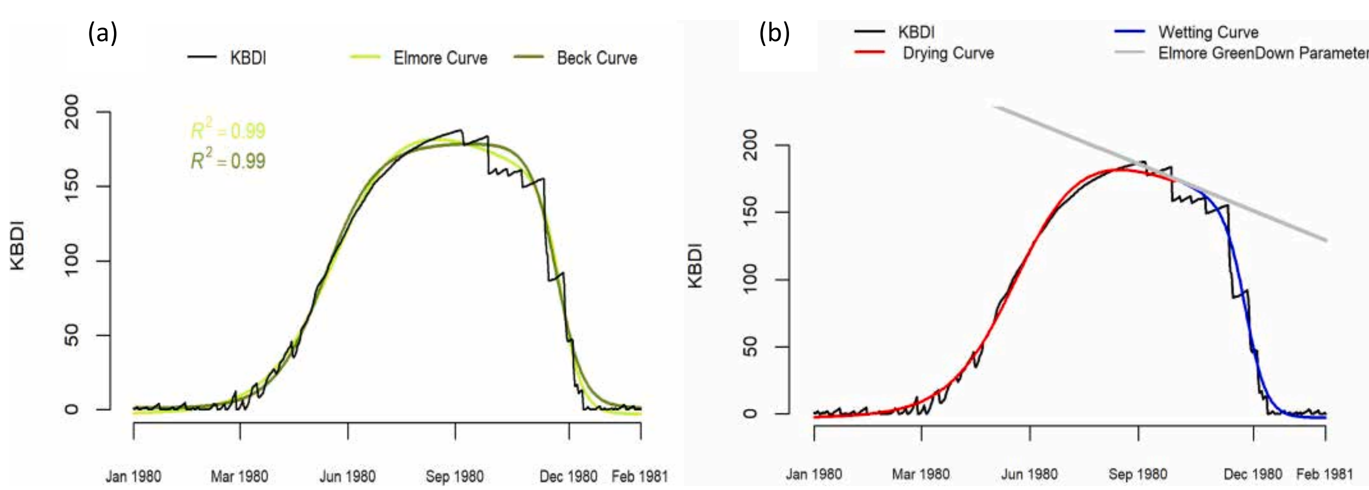

Fig. 2. a) Beck (dark olive green, 6-parameter equation) and Elmore (light olive green, 7-parameter equation) fine fitting curves and corresponding goodness of fit (R-squared) b) Elmore dual logistic curves, with the drying curve (red) represents soil moisture depletion, while the wetting curve (blue) signifies soil moisture replenishment. (For interpretation of the references to colour in this figure legend, the reader is referred to the web version of this article.)

(RP.SD) (in mm).

In addition to all of these features, and while the topic of “Flash Drought” is rapidly gaining attention within the research community on drought impact assessment (Otkin et al., 2018), we identified a drought feature representing the intensification rate between the lowest and highest (i.e., extreme) onset level (Iglesias et al., 2022). However, we do not attempt to propose a definition of ‘Flash Drought” nor assess its behavior within the ongoing discourse about its various definitions, whether it is perceived as a rapid-onset of drought or as a short-term, yet severe drought event (Lisonbee et al., 2022). At present, there is no standard definition or formula to calculate drought intensification rates, but it is usually defined as the measurement of increases in drought intensity over a specified time period (Liu et al., 2020). We calculated a drought intensification rate, hereafter called “Drying Rate”, as the slope of the tangent to the drying curve at its inflexion point. In a similar manner, we calculated the “Wetting Rate” over the wetting curve, a numerical rating on the rate of soil moisture replenishment after reaching the driest days.

We ended up with 19 features (Table 1) characterizing the daily reconstructed KBDI time series over each hydrological year, so that each year can be considered as an individual, characterized and described by its own drought features (Fig. 3). In addition, the 19 extracted drought features encompass the multi-stage drought concept, recently proposed by Bonsal et al (2011), who have split the development and recovery drought stages into six different periods, namely “onset”, “growth”, “persistence”, “peak”, “retreat”, and “termination”.

2.4.3. Drought characterization under semi-arid and arid conditions

We constructed 19 drought features on the premise that, under humid and sub-humid climates with a yearly rainfall amount ranging between 800 and 1400 mm (i.e., coastal zones and western mountainous ranges in Fig. 1a), the soil will be replenished and saturated to its field capacity at the end of the dry season. In such instances, we can identify two specific points within the time series, from initial deviance to the return to field capacity, further used to extract the previously mentioned drought features within the hydrological year (Fig. 4). However, under semi-arid and arid conditions characterized by a rainfall pattern ranging between 200 and 600 mm (e.g., Baalbek-Hermel and Bekaa Governorates in Fig. 1a), it is not always the case that the soil moisture reaches field capacity at the end of each hydrological year, or even reaches our lowest drought threshold of KBDI-50 or the moderate threshold of KBDI-100 (Fig. 5). In these regions, we may observe prolonged drought events for each threshold level that can last over many years to decades called hereafter “Multi-Year Droughts”, continuing until reaching the next soil saturation threshold level (Tsakiris et al., 2010; Xu et al., 2021).

In such cases, we then had to consider consecutive hydrological years until reaching our predefined thresholds and extract drought features when they were missing in a single hydrological year. First, we identified how many years the KBDI-50, KBDI-100, and KBDI-150 thresholds have not been reached. Within this Multi-Year Drought period (MYD), we determined the hydrological years as delimited by the minimum KBDI value and its corresponding day since beginning (i.e., DOY since 1960, 1st January) between two successive years driest peaks (Peak.KBDI.DOY). This minimum value signifies insufficient precipitation to restore soil moisture to its field capacity for the corresponding hydrological year, and at the same time it marks the end of the current hydrological year with re-increasing of KBDI following first dry spells, even when not having fully replenished the soil to field capacity. We then characterized the missing features of these years included within prolonged drought spells.

For a given year n not reaching one of the KBDI threshold at the end of the hydrological year, we assigned the end of the dry season D.offset at this KBDI threshold as the number of days since January 1st of this year n when the KBDI threshold is finally reached, would that be at year $n + 1$ or later. This value is then higher than 366 and can reach very high values. Let’s note also that, for example a 4-year prolonged drought covering years $n, n + 1, n + 2, n + 3$ (Fig. 5), the drought offset (D.offset) of year $n + 1$ would be the number of days spanning between January 1st of this year ($n + 1$) and when the KBDI threshold is reached, and D. offset of year $n + 2$ would be the number of days spanning between January 1st of the year $n + 2$ and when the KBDI threshold is reached. For this similar 4-year drought, drought onset date (D.onset) of year n would be calculated as a normal year, while D.onset of year $n + 1$ would be a negative value, counting the number of days before January 1st of the $n + 1$ when the drought started during year n. D.onset of the year $n + 2$ would be also a negative value, counting the number of days before January 1st of the $n + 2$ when the drought started during year n, thus being D.onset $n + 1$ – 365. We then derived drought duration DD and drought severity DS, not based on D.onset and D.offset as previously performed for sub-humid conditions, as we aim at quantifying drought features describing soil desiccation affecting agro-ecosystem functioning of the current year n, thus omitting whatever happens after this

Table 1
Drought features abbreviations, units, and corresponding descriptions.

Drought Features	Abbreviations	Units	Description
Low Drought Onset	Low.D.Onset	DOY	Soil moisture reaching 75 % of its AWC
Moderate Drought Onset	Moderate.D.Onset	DOY	Soil moisture reaching 50 % of its AWC
Extreme Drought Onset	Extreme.D.Onset	DOY	Soil moisture reaching 25 % of its AWC
Low Drought Offset	Low.D.Offset	DOY	Soil moisture recovered to 75 % of its AWC
Moderate Drought Offset	Moderate.D.Offset	DOY	Soil moisture recovered to 50 % of its AWC
Extreme Drought Offset	Extreme.D.Offset	DOY	Soil moisture recovered to 25 % of its AWC
Low Drought Duration	Low.D.Duration	Days	Period spanning between Low Drought Onset & Offset
Moderate Drought Duration	Moderate.D.Duration	Days	Period spanning between Moderate Drought Onset & Offset
Extreme Drought Duration	Extreme.D.Duration	Days	Period spanning between Extreme Drought Onset & Offset
Low Drought Severity	Low.D.S	mm/day/year	KBDI sum between Low Drought Onset & Offset
Moderate Drought Severity	Moderate.D.S	mm/day/year	KBDI sum between Moderate Drought Onset & Offset
Extreme Drought Severity	Extreme.D.S	mm/day/year	KBDI sum between Extreme Drought Onset & Offset
Peak KBDI	Peak.KBDI	mm	Maximum KBDI value observed over the hydrological year
Peak KBDI Day Of the Year	Peak.KBDI.DOY	DOY	Day of the year when KBDI reaches its peak value
Drying Rate	Drying.rate	mm/day	Maximum daily soil water loss derived as the slope of the tangent to the drying curve at the inflection point
Wetting Rate	Wetting.rate	mm/day	Maximum daily soil water recovery derived as the slope of the tangent to the wetting curve at the inflection point
Rainfall Pulses numbers	RP.num	Number	Rainfall Pulses numbers between Peak.KBDI.DOY and Extreme.D.Offset
Rainfall Pulses mean Intensity	RP.I.mean	mm	Mean Intensity of Rainfall Pulses
Rainfall Pulses Standard Deviation	RP.SD	mm	Rainfall Pulses Standard Deviation

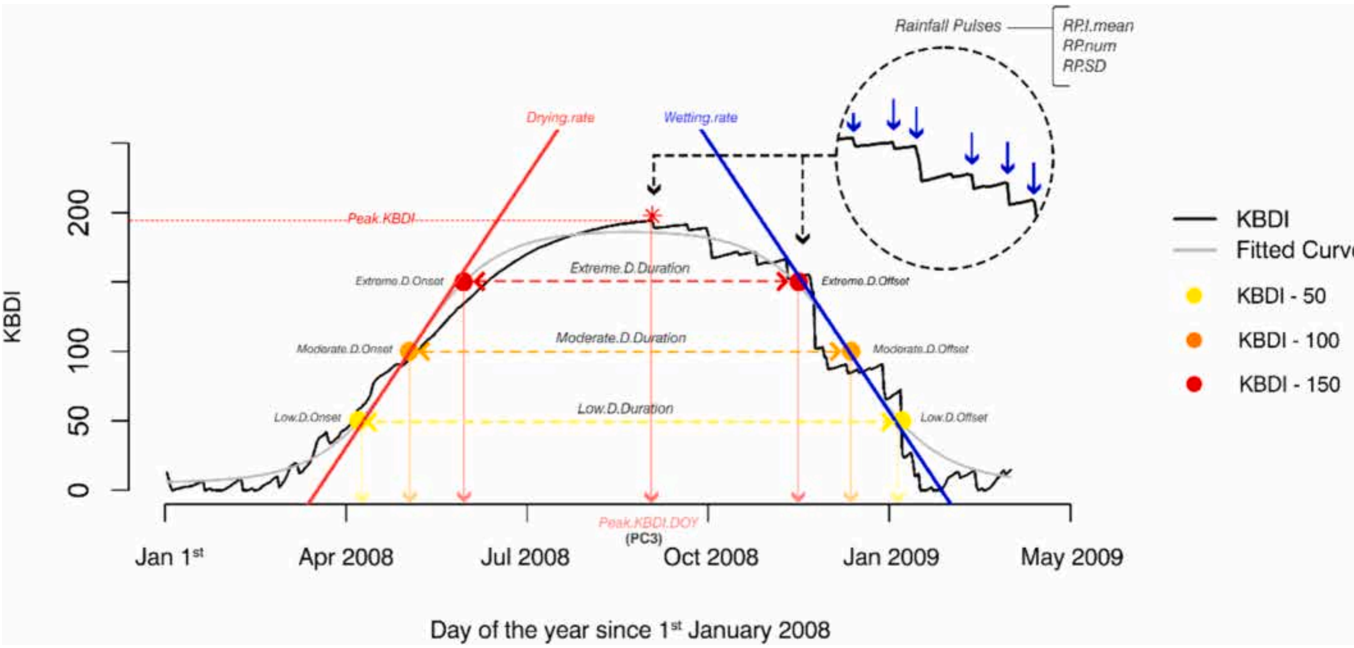

Fig. 3. Drought features derived from KBDI daily values of a hydrological year (from Day of the Year 1 to 420). Low.D.Duration: Low Drought Duration; Moderate.D.Duration: Moderate Drought Duration; Extreme.D.Duration: Extreme Drought Duration; Peak.KBDI.DOY: Day of the year featuring the highest KBDI value; Peak.KBDI: Peak KBDI Value; Extreme.D.Offset: Extreme Drought Offset; Low.D.Offset: Low Drought Offset; Moderate.D.Offset: Moderate Drought Offset; RP.I.mean: mean intensity of Rainfall Pulses; RP.num: Rainfall Pulses number; RP.SD: Rainfall Pulses Standard Deviation; Low.D.Onset: Low Drought Onset; Moderate.D.Onset: Moderate Drought Onset; Extreme.D.Onset: Extreme Drought Onset.

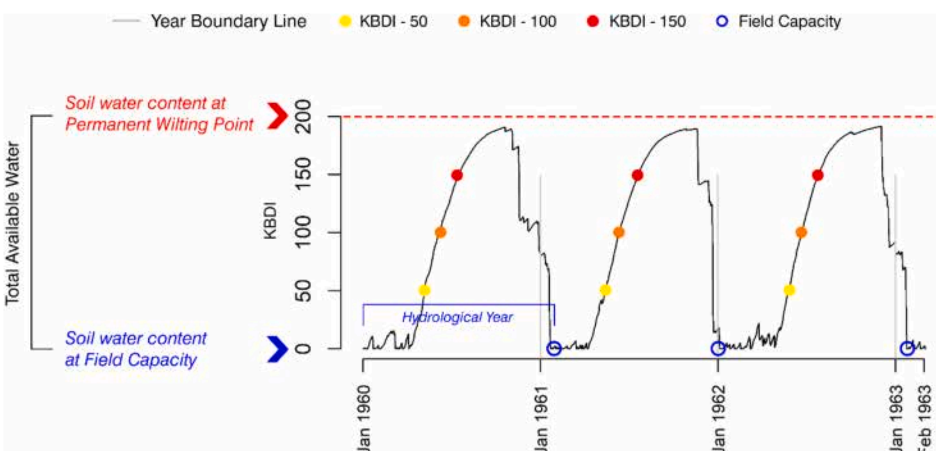

Fig. 4. KBDI time series over 3 hydrological years starting January 1st 1960. End of hydrological years (blue circles), year boundaries (vertical gray lines) and day of the year (DOY) when reaching KBDI thresholds (KBDI-50 yellow dots, KBDI-100 orange dots, and KBDI-150 red dots) are represented. Hydrological years span between January 1st (gray vertical lines) and the first day when soil is replenished to its field capacity (blue circles) after the seasonal drought. (For interpretation of the references to colour in this figure legend, the reader is referred to the web version of this article.)

hydrological year. DD (and DS) of year n were then calculated as the number of days (sum of KDBI) between D.onset of year n and DOY of the minimum KBDI value between the year n and $n+1$. This way, within a 4-year prolonged drought event, all the years will have the same difference between D.onset and D.offset, but only the last year (year $n+3$) will truly experience this prolonged drought regarding its functioning.

As a result of this conceptualization, we could characterize three typical Mediterranean drought dynamics (drought-types) covering the climatic gradient of Lebanon, namely, MED, HMED, and DRY-MED (Fig. 6). MED represents a typical Mediterranean soil moisture dynamic surpassing (and recovering) the three defined soil desiccation thresholds KBDI-50 (low), KBDI-100 (moderate), and KBDI-150 (extreme) during the dry season. HMED represents a Mediterranean humid dynamic not reaching low, moderate, or extreme soil desiccation thresholds at its driest day, while DRY-MED represent an arid dynamic with a Multi-Year Drought (MYD) pattern when the wet season KBDI values remain over the low, moderate, or extreme KBDI thresholds.

2.4.4. Multivariate drought features analysis

We reached 19 drought features over hydrological years, based on critical soil desiccation levels targeted to significantly affect agro-ecosystem functioning. A Principal Component Analysis (PCA) was performed using the 'FactoMineR' and 'factoextra' R-cran packages to reduce the dimensionality of the data into a smaller set of uncorrelated variables that capture the directions and informative aspects of maximum variance in the original data (Kassambara, 2016; Lê et al., 2008). Accordingly, the original intercorrelated drought features will be reduced to new linearly uncorrelated ones, to distill the essential

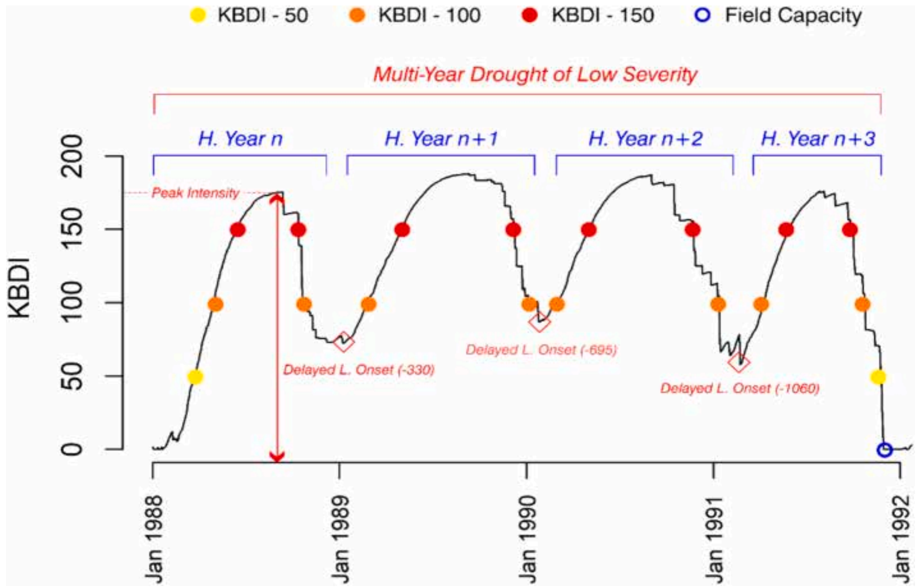

Fig. 5. KBDI variations within a Multi-Year Drought event under semi-arid and arid conditions. A prolonged Multi-Year Drought of low severity (yellow dots) is depicted over four consecutive hydrological years. Each encompassed year within the prolonged event is distinguished by its unique drought features. Red negative numbers denote the delayed onset of the current year's drought, based on the conditions of the previous year. Drought severity and duration are cumulatively calculated over subsequent hydrological years. (For interpretation of the references to colour in this figure legend, the reader is referred to the web version of this article.)

information from them. At the same time, and in order to understand the intricate relationships between drought features, correlation matrices following a hierarchical clustering were generated offering an opportunity for a quantitative comparison of associations between pairs of the extracted drought features. For the PCA, the variables were standardized, thus experiencing a standard deviation of one and a mean of zero, to account for differences in measurement scales, rendering the variables comparable. Accordingly, the Principal Components (PCs) are computed in a decreasing order of importance. Based on the eigenvalues, which quantify the amount of variation preserved by each component, we have identified the number of PCs to be considered (Santos et al., 2010; Sharma, 1995). The entire methodological development for the automated model development, including subsequent analyses, was carried out using R (v4.2.2) (Core Team, 2021).

3. Results

3.1. Biogeography of drought types along the aridity gradient in Lebanon

As a first step, we aimed at using DFEAT to characterize the biogeography of drought types across the study region based on how KDBI could reach the soil desiccation thresholds and be refilled to a KBDI of zero (soil water content at field capacity) during the winter period. Fig. 7 then represents the fraction, for each 9x9 km ERA5-L pixel, of hydrological years experiencing either i) a typical Mediterranean (MED) soil moisture dynamic (Fig. 7a-c), ii) a Mediterranean humid (HMED) dynamic (Fig. 7d-f), or iii) an arid dynamic (DRY-MED) with a Multi-Year Drought (MYD) pattern (Fig. 7g-i).

We first observe that, over the Lebanese aridity gradient, 55.64 %, 71.77 %, and 75 % of the territory experience more than 95 % of years with of MED-type soil moisture dynamic reaching during the winter period respectively the low, moderate, and extreme severity drought thresholds, mostly located on the coastal zone. This regional pattern follows the precipitation and temperature gradients of the region (Fig. 1a), suggesting a reliable representation of drought from our indices.

When looking at the regions where non-MED drought types significantly occur, we observe that the Northeastern region near the Syrian border where low annual precipitations occur, experiences DRY-MED drought-type. Numerous MYD events get more frequent from the Beqaa Valley to the Syrian border and reach 90 % of the years experiencing MYD, at the low and moderate thresholds (Fig. 7g, h). No such DRY-MED-type events were observed at the extreme threshold anywhere over the Lebanese territory (Fig. 7i), meaning that all regions in Lebanon get enough winter rainfall to refill 25 % of the 203 mm field capacity. Finally, when looking at the HMED drought type years (not reaching a sufficient soil desiccation threshold during summer), we observe that they only occur for the extreme threshold and represent 100 % of the non-MED-drought-type years over Mount-Lebanon and Anti-Lebanon for this threshold (Fig. 7f). By covering the Lebanese aridity gradient representative of the Mediterranean basin, we show here that our method is able to capture the regional distribution of various drought-types, and could cover 100 % of cases during the 1960–2020 period.

3.2. DFEAT drought features variations in Mediterranean and humid conditions

Based on the biogeographical distribution of drought types, we then explored separately the drought features generated across the 26 pixels along the coastal line (MED-type droughts) and across the 16 pixels located in the more humid mountainous region of Mount-Lebanon (HMED-type droughts) over the period 1960–2020 (Table 2). In these regions, DFEAT could estimate that drought onsets (Low.D.onset) varied between DOY 135 $\pm$ 14.17 (May 15th) in the coastal area and 168 $\pm$ 16.44 (June 16th) in the mountainous areas for a KBDI threshold of 50. We observed on average a 30-day delay in the Mountains for KBDI-50 and KBDI-100, while reaching a 45-day delay for the KBDI-150 extreme threshold, thus starting on day 237 (August 25th). During this drought onset period, the drying rate (Drying.rate) was faster on the coast at 2.04 mm/day, while it reached only 1.68 mm/day in the mountains illustrating the slower soil desiccation rate under lower temperatures at high altitudes.

Drought offset dates of year *n's* varied between 373 $\pm$ 24.63 (January 8th of the year $n + 1$) in the coastal area and 378 $\pm$ 27.06 (January 13th of the year $n + 1$) in the mountainous areas for a KBDI

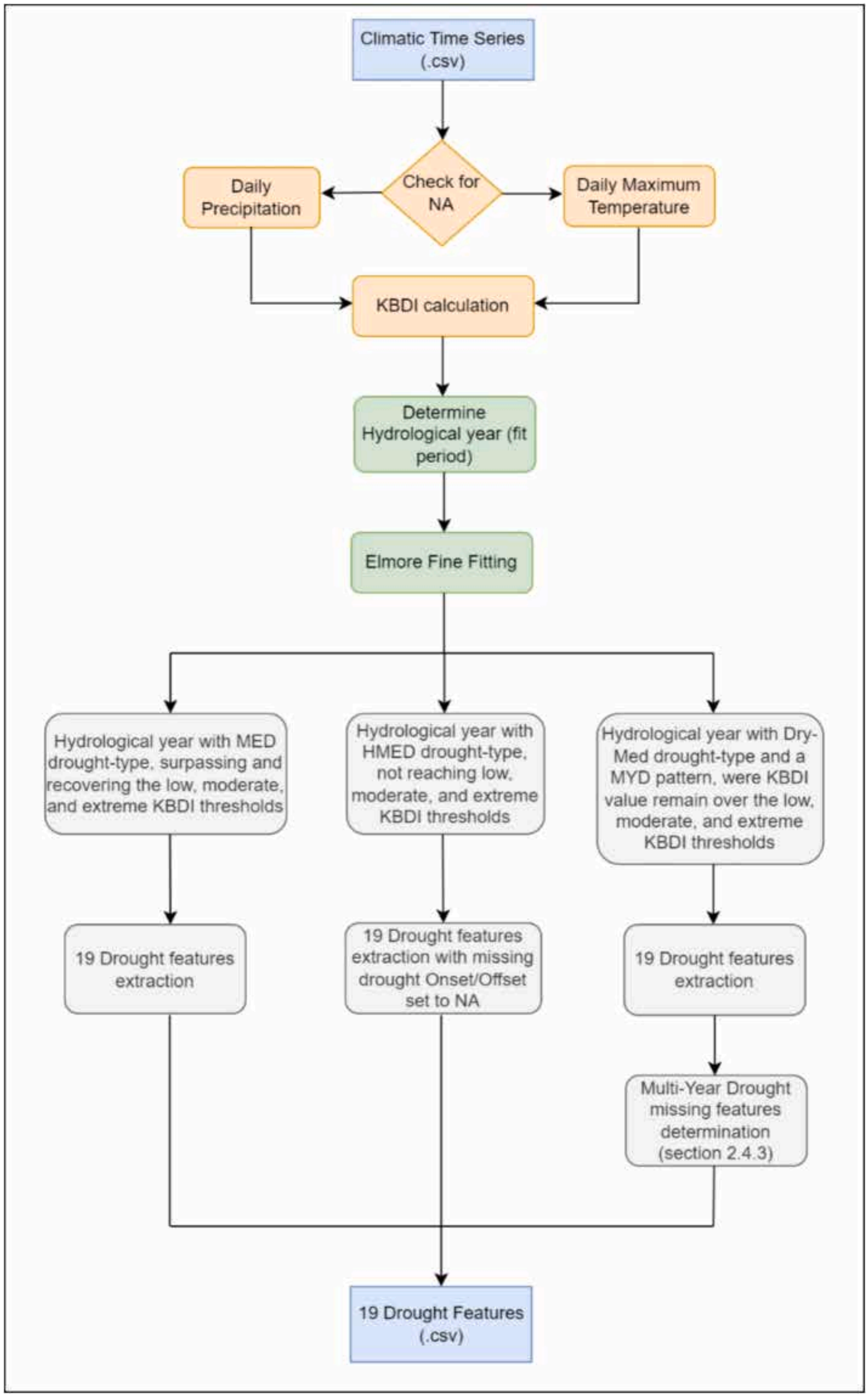

Fig. 6. Flowchart of the successive steps implemented in DFEAT in order to extract yearly drought features from daily calculated KBDI time series. The blue rectangles symbolize both the model input and output. The orange rounded rectangles depict the process involved in climatic data processing and KBDI calculation. The green elements represent the fitting process. Meanwhile, the gray rounded rectangles illustrate the procedures for extracting drought features along the climatic gradient of Lebanon. (For interpretation of the references to colour in this figure legend, the reader is referred to the web version of this article.)

threshold of 50, illustrating the end of the dry season of year *n* to happen late in the winter season in January of year $n + 1$. We observe a very small difference in drought offset DOY (for both the low and moderate drought levels), between the coastal area and the wettest mountainous area, a major difference compared to the regional pattern of drought onset DOY, mostly due to large scale rainfall events in winter refilling the soils. However, the offset of the extreme drought level KBDI-150 is earlier by 11 days in the mountainous area (November 20th) compared to the coast (December 1st) where winter rainfalls may happen later or soil water content was more fully desiccated under higher temperatures. Drought offset dates also experience a higher interannual variation with SD varying between 17 days and 27 days according to the KBDI threshold, compared to 13–21 days observed for the drought onset. During that drought offset period, the wetting rate was faster on the

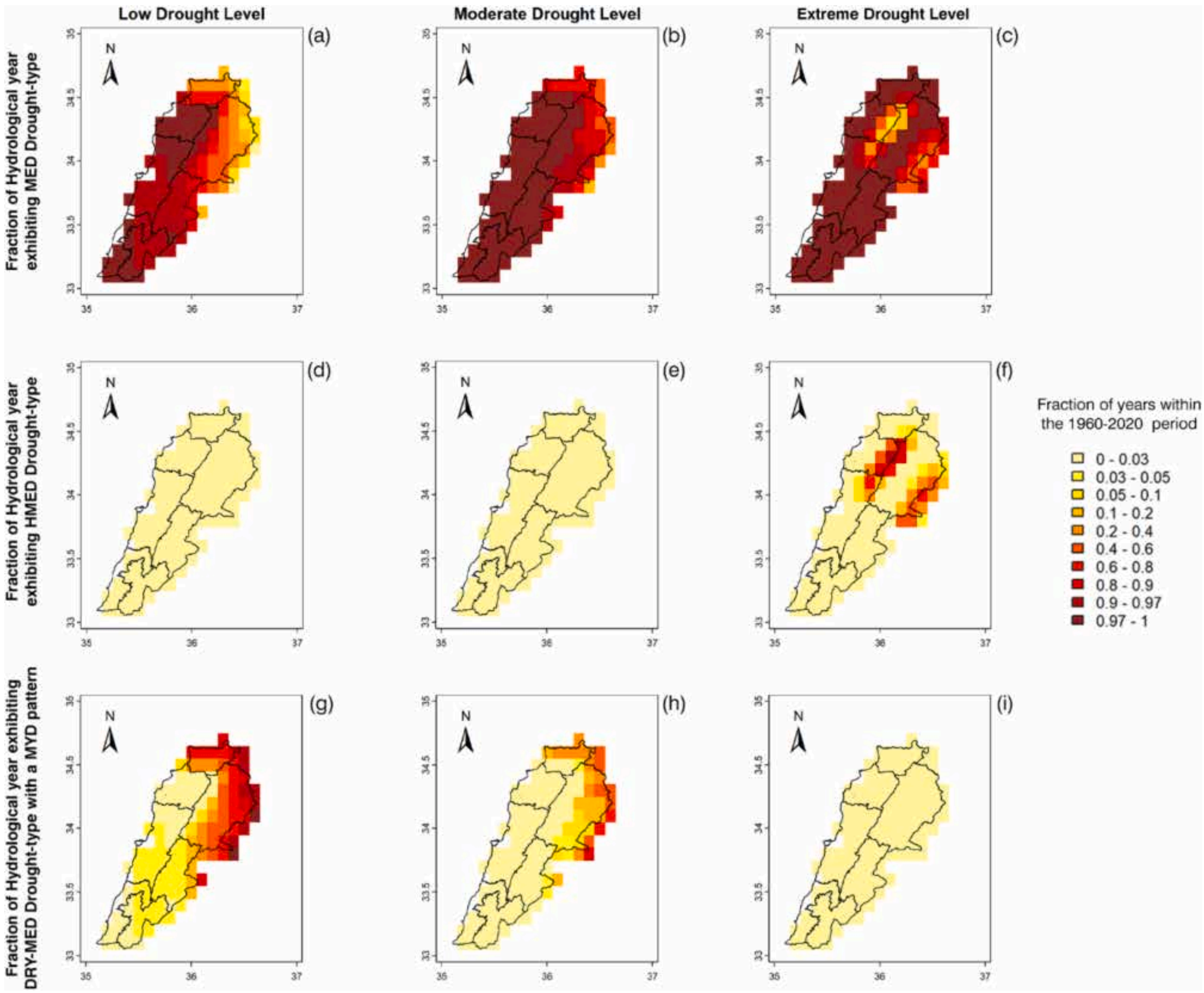

Fig. 7. Fractions of hydrological years over the 1960–2020 period characterized by different soil moisture dynamics representative of typical Mediterranean conditions. These dynamics include a typical Mediterranean soil moisture dynamic (MED) drought-type (a–c), a Mediterranean humid (HMED) drought-type (d–f), and a Multi-Year Drought pattern (DRY-MED drought-type) (g–i) across varying levels of low, moderate, and extreme soil desiccation thresholds.

Table 2
The mean and standard deviation (SD) of the extracted drought features in two distinct climatic zones: the coastal zone and the humid western mountainous zone of Lebanon.

Drought Features	Mean (1)	SD (1)	Mean (2)	SD (2)
Low Drought Onset	135.80	14.17	167.79	16.44
Moderate Drought Onset	163.37	13.59	198.60	15.99
Extreme Drought Onset	192.50	14.03	237.31	20.59
Low Drought Offset	373.90	24.63	378.99	27.06
Moderate Drought Offset	356.51	21.02	355.78	25.70
Extreme Drought Offset	335.33	17.02	324.47	22.93
Low Drought Duration	237.58	29.70	209.98	35.47
Moderate Drought Duration	193.92	26.27	157.02	34.60
Extreme Drought Duration	142.83	23.71	43.39	50.47
Low Drought Severity	33662.64	4483.63	24650.16	5215.6
Moderate Drought Severity	30648.96	4567.25	21222.67	5856.31
Extreme Drought Severity	24704.79	4500.66	7009.17	8250.51
Rainfall Pulses number	4.65	2.29	1.58	2.39
Rainfall Pulses mean Intensity	17.86	15.18	3.35	5.43
Peak KBDI	190.05	4.45	158.36	12.60
Peak KBDI DOY	293.64	15.44	294.45	16.11
Drying Rate	2.041	0.212	1.68	0.15
Wetting Rate	−4.21	3.38	−2.72	2.19

SD = Standard Deviation, (1): Coastal Zones, (2): Higher Western Mountains.

coast at – 4.21 mm/day compared to −2.72 mm/day in the mountains, as a consequence of more numerous rainfall pulses on the coast (4.65 ± 2.29 events) compared to the mountains (1.58 ± 2.39 events) with much more intense events, 17.86 (±15.18) mm compared to 3.35 (±5.43) mm.

In turn, drought duration varied between 142 (±23.7) days for extreme KBDI-150 drought level to 237 (±29.70) days for the low KBDI-50 drought level in the coastal area, and was respectively reduced by 99 days and 28 days in the mountains. Similarly, drought severity varied between 24.7 10^3 mm to 33.7 10^3 mm and was reduced to 7.009 10^3 mm and 24.6 10^3 mm in the mountainous area.

Within this drought duration period, the peak drought date was very similar between the two zones, with DOY=293 (±15.44) (October 20th) in the coastal area and DOY = 294 (±16.11) (October 21th) in the mountains. The peak KBDI value was however higher in the coastal zone reaching 190 (±4.45) mm of soil desiccation compared to 158 (±12.60) mm in the mountainous region, thus potentially hardly reaching the 150 mm threshold as observed in Fig. 7f.

3.3. DFEAT assessment over Multi-Year-Droughts under arid conditions

We analyze here the ability of DFEAT to capture and describe the particular case of Multi-Year Droughts observed under DRY-MED-drought types located on 42 pixels of the Northeastern part of Lebanon (Fig. 7g and h) in the governorates of Baalbek-Hermel and Bekaa with an annual precipitation less than 600 mm.

Table 3 presents the drought features generated by DFEAT over the pixels with more than one MYD event (Akkar and Baalbeck-Hermel governorates). For this particular case of MYD, DFEAT generates a mean DOY of low drought onset of −388.18 with a high standard deviation of 926.03 days, illustrating that, for a given year *n* starting on January 1st, KBDI values below the KBDI-50 threshold started during the early days of year *n-1*. This can vary between 2.5 years (926 days) and can even reach for the driest area 23 years (Fig. 8) out of our 60-year period (1960–2020). The mean values of DOY drought onset for KBDI-100 and KBDI-150 are positive values reaching respectively DOY = 93 and DOY = 202, but with a standard deviation SD = 252.67 higher than the mean for KBDI-150, showing that drought onset can reach negative values for the moderate KBDI threshold with MYD drought events. For the KBDI-150 threshold, SD = 26.60, a low value suggesting that no MYD events are observed at this threshold and that soil water content is partially refilled every year.

During that drought onset period, the drying rate was 1.44 ± 0.35 mm/day, slightly less than the drying rate observed in coastal zones dominated by MED drought types as a consequence of partial soil drying so that desiccation dynamic is mostly controlled during stomatal closure included in KBDI calculations. Drought offset DOY for the lower KBDI-50 and moderate KBDI-100 thresholds reaches much higher values than under MED or HMED conditions, respectively DOY = 1087.23 and DOY = 482.63, with similarly high SD of 1113.92 days and 272.69 days. This indicates that MYD events in this region end up on average 3 years after their onset, but can reach more than 6 years for the KBDI-50 threshold, while end up on average 1.5 years after onset and vary up to 2.5 years for the KBDI-100 threshold. This leads to an extended drought duration in regions where MYD are observed, reaching up to 8300 days (23 years) for KBDI-50 at the driest site, 2835 days for KBDI-100, and less than 365 days for the extreme KBDI-150 threshold, so that no MYD are observed for this threshold (Fig. 8). During that drought offset period, the wetting rate was −1.92 mm/day, twice less than the value observed over the coastal zone as a consequence of less intense storms. The Peak KBDI value is 178.23 (±14.20) mm, falling between the Peak KBDI values of the coastal and mountainous zones and is reached at DOY = 298 (±18.81) (October 25th).

3.4. Sensitivity of drought features to temperature

While illustrating that DFEAT was able to produce drought features for all drought-type years across the climatic gradient in the region, we tested the sensitivity of drought features when varying the daily maximum temperature (Fig. 9), representing the potential variation of temperature within the 9 km pixel due to elevation considering a generic lapse rate of −0.66 °C for a 100 m increase in altitude. A decrease of two degrees in the daily maximum temperature resulted in a delayed onset of 7.3 %, 6.4 %, and 8.8 %, and an earlier offset of −1.6 %, −1.8 %, and −2.2 % for the low, moderate, and extreme drought levels, respectively. Conversely, a two-degree rise in daily maximum temperature resulted in an earlier onset of −6.2 %, −7.2 %, and −6.7 %, and a delayed offset of 1.2 %, 1.10 %, and 1.16 % for the low, moderate, and extreme drought levels, respectively. This in turn, would result in a more severe and prolonged drought period than usual, with an increase of 5.6 %, 8 %, and 13 % for the low, moderate, and extreme drought levels, respectively. Additionally, it is characterized by a substantial increase in drying rate (i.e., the propagation from low to extreme drought severity) and an earlier peak of KBDI values in the season as a consequence of increase evapotranspiration in KBDI calculations. These results highlight the sensitivity of DFEAT to temperature uncertainties or potential impact of climate change.

Table 3
Mean and Standard Deviation of the extracted Drought features for Multi-Year Drought events.

Drought Features	Mean	Standard Deviation
Low Drought Onset	−388.18	926.03
Moderate Drought Onset	93.18	252.67
Extreme Drought Onset	202.94	26.60
Low Drought Offset	1087.23	1113.92
Moderate Drought Offset	482.63	272.69
Extreme Drought Offset	357.28	31.66
Low Drought Duration	859.28	994.72
Moderate Drought Duration	316.36	276.60
Extreme Drought Duration	140.43	63.42
Low Drought Severity	117,166.7	140,739.5
Moderate Drought Severity	47,621.28	43,084.73
Extreme Drought Severity	23,827.33	11,261.2
Rainfall Pulses number	5.98	3.66
Rainfall Pulses mean Intensity	6.90	5.87
Peak KBDI	178.23	14.20
Peak KBDI DOY	298.05	18.81
Drying Rate	1.44	0.35
Wetting Rate	−1.92	1.38

3.5. Interdependencies and dimensionality reduction of drought features

Finally, we tested whether our 19 drought features are independently meaningful, or highly correlated, so that they could be reduced to few keystone ones. We performed two PCA analysis for the whole country and for the MED/HMED region, to retain the first six components which explain 90 % of the original data (Fig. 10a and b). We observed that moderate drought duration/severity and drying rate were the primary features driving PC1 (52 % of the variance) and PC2 (21 %) respectively. PC3 (7.5 %) and PC4 (5.3 %) are represented by peak drought day and rainfall pulses mean intensity, respectively, while PC5 (4.4 %) and PC6 (3.1 %) are represented by extreme drought onset and wetting rate, respectively. However, in regions with a typical MED and HMED drought dynamic (Fig. 10b), the order of representation of drought features across the six dimensions differs, with only the first dimension PC1 consistently represented by moderate drought duration and severity (40 % of variance explained). Drought Onset (Low and Moderate) are captured in PC2 (21.6 % of the variance). PC3 (9.6 %) and PC4 (7.4 %) are represented by Wetting Rate and Rainfall pulses number, respectively. PC5 (5.5 %) and PC6 (4.5 %) dimensions are mainly represented by Drying Rate and Rainfall pulses mean intensity, respectively.

We conclude here that, based on a daily water balance model, at least 6 independent features can characterize a drought event, much higher than the usually assessed drought severity/duration and thus offering a new multifaceted characterization to explain agro-environmental issues.

4. Discussion

4.1. DFEAT operationality assessment

While the severity and duration of drought have garnered the utmost attention among all drought dimensions in regional- to global-scale drought studies (Gao et al., 2018), our drought feature assessment tool DFEAT aims at providing a generic processing chain to capture keystone additional information from a daily time series of soil desiccation (tested here with the widely used KBDI drought index). Based on user needs for characterizing daily soil desiccation into synthesized yearly agro-meteorological indices (onset, development/drying, persistence, peak and recovery/rewetting, and offset) for different levels of KBDI thresholds within a dry spell (Bonsal et al., 2011; Oukaddour et al., 2024), we ended up with 19 drought features, including three soil desiccation thresholds. Large scale validation of DFEAT indices would not be possible as assuming a constant soil field capacity, and coarse resolution climate inputs. We synthesized however drought characteristics previously stated for the region and compared to our estimates.

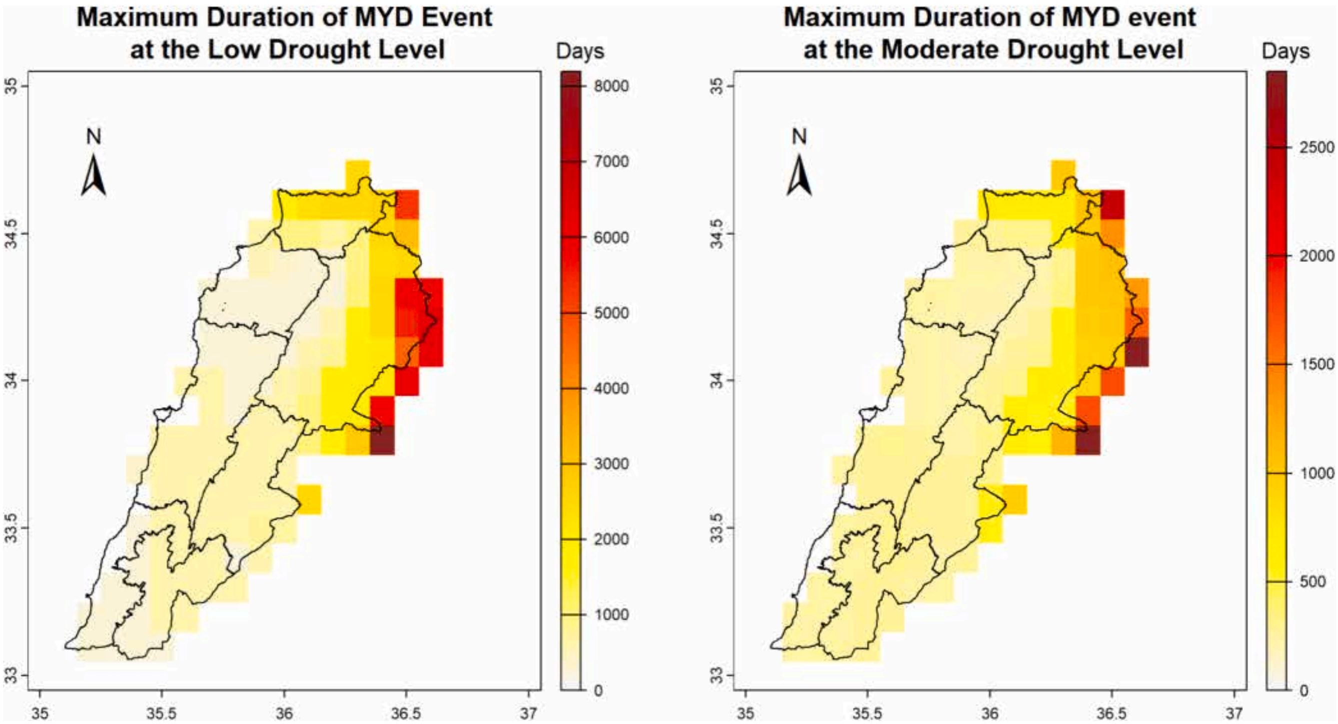

Fig. 8. Maps of maximum duration (in days) of MYD events for the low and moderate KBDI thresholds along the climatic gradient in Lebanon.

Among these features, we have identified the first day that reaches the driest value (i.e., highest KBDI values, Peak.KBDI) as the peak drought day (Peak.KBDI.DOY). DFEAT yielded an average peak drought day value of 293 ± 15.44 DOY (October 20th) on coastal zones and 298 ± 18.81 (October 25th) on semi-arid and arid zones. These results are consistent with Mediterranean conditions, where the driest day over the year typically occurs in late summer and early fall (Vogel et al., 2021). In Lebanon, the summer season is warm and dry, spanning from June to October, and characterized by scarce and almost no precipitation, with September being the less watered of the year (Kobrossi et al., 2021). From a climate-alone perspective, this day may coincide with the end of a period holding the lowest accumulated precipitation and when PET is highest (Ferijal et al., 2022). Our average driest peak DOY values also align with the highest PET observed during the prolonged dry spell in Lebanon (Allam et al., 2021). This driest peak DOY may persist up to the mid-fall season, until November 3rd (coast) and November 12th (semi-arid/arid zones), in line with previous studies conducted in the region. Majdalani et al (2022) identified, on average, maximum soil drought conditions during the month of October, reaching November for some extreme years by using the Fire Weather Index (FWI) drought Code (DC), while Salloum and Mitri (2014), mentioned a peak of the dry (fire) season around November 12th. DFEAT then provided consistent values of Peak drought DOY for the region. The driest day of the year is close to the drought offset under Mediterranean climate where drought offset is usually associated with heavy storms filling up the soil to field capacity in one single event when soil is the driest (Singh et al., 2021).

The number of rainfall pulses (Rp.num) during the stability (persistence) phase (between peak KBDI DOY and extreme drought offset) was also calculated, along with its magnitude (RP.I.mean) in mm and standard deviation (RP.SD) for each hydrological year. DFEAT estimated an average number of rainfall pulses of 4.65 ± 2.29 events over coastline zones and 1.58 ± 2.39 over the higher western mountains, with intensities of 17.86 ± 15.18 mm and 3.35 ± 5.43 mm, respectively. This feature is actually hardly quantified and assessed in hydrological studies, although soil moisture increment pulses (Collins et al., 2014; Manzoni et al., 2020) have been defined and their intensity and frequency identified as keystone features related to hydrological and ecological processes (Loik et al., 2004). Our estimates of 17.86 mm for pulse intensities in the coastal zone of Lebanon is in accordance with the 25 mm rainfall pulse experimentally simulated by Barnard et al (2015), 20 mm as reported by Vargas et al (2012), and 15 mm according to Pockman and Small (2010). We'll note that this feature is actually closely related to the 'green down' parameter of the Elmore curve, that we chose to replace by this more hydrologically meaningful information and prevent redundancy.

The rate of soil desiccation (i.e., Drying.rate) and soil moisture recovery after seasonal drought (i.e., Wetting.rate) have been also calculated for each hydrological year (Fig. 3). Both features represent novel characteristics in the field of drought monitoring that have recently emerged (Otkin et al., 2018), with only few attempts using precipitation/evapotranspiration indices such as SPEI calculated on one-month window (Iglesias et al., 2022; Lisonbee et al., 2022), and soil moisture indices (Han et al., 2023; Liu et al., 2020; Qing et al., 2023). Rainfall pulses are integrated in this wetting rate, smoothed over the wetting curve, a rarely assessed drought feature in hydrological studies, yet potentially significant for agro-ecological functioning (Collins et al., 2014; Dodd et al., 2015; Manzoni et al., 2020).

DFEAT could retrieve the timing of drought occurrence (onset and offset), duration, and severity. For the low drought level; an onset DOY in mid-spring (May 15th) and early summer season (June 16th) over coastal zones and higher wettest mountains, respectively. A moderate and extreme drought onset has also been determined for the coastal zones (June 12th, July 11th) delayed by roughly one month in mountain zones (July 17th, August 25th). These estimations align with prior research conducted in the Mediterranean basin (Barbeta and Peñuelas, 2016; González-Hidalgo et al., 2018; Lempereur et al., 2017, 2015; Majdalani et al., 2022; Ruffault et al., 2013; Zribi et al., 2016), with drought onsets occurring between (DOY = 145) May 25th and (DOY = 239) August 28th, with delays over the wettest mountainous areas, with an average value of 210 DOY (July 29th). DFEAT retrieves approximately the same average drought offset for the low (January 8th, January 13th of the year $n + 1$) and moderate (December 22th, December 21th) drought levels in the coastal zones and wettest mountains, respectively. This offset is earlier by 11 days in the wettest

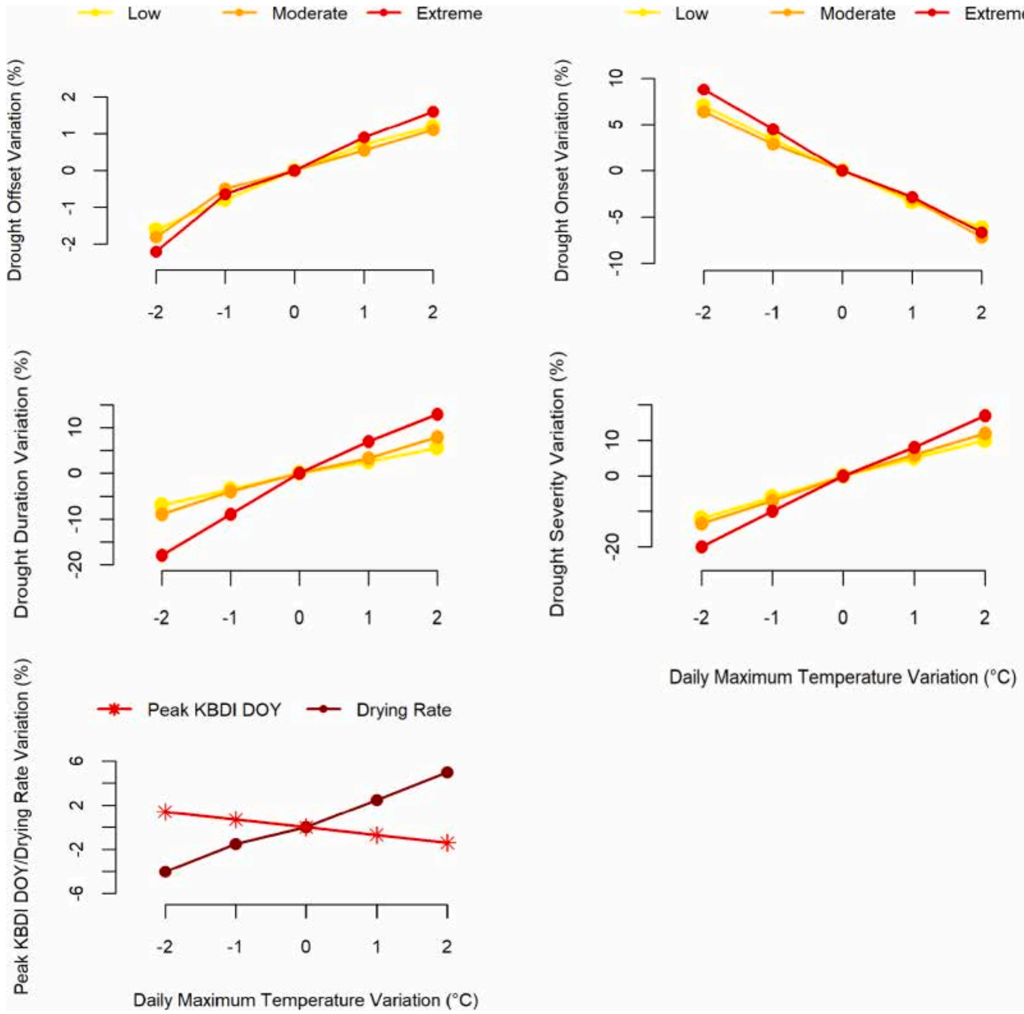

Fig. 9. Drought Features sensitivity to various scenarios of daily maximum temperature changes. The value of "0" indicates no changes, while "−2" and "+2" represent a decrease and an increase of two degrees Celsius in daily maximum temperature, respectively.

mountains (November 20th) compared to coastal zones (December 1st) for the extreme drought level. Our observations are slightly higher than those observed by Ruffault et al (2013) in southern France, who found drought offsets varying between August 19th and November 7th and Zribi et al (2016) who found an average drought offset around mid-December (varying between DOY 320 and 370) in Tunisia. The observed difference in our drought offset can be primarily attributed to the particular precipitation regime in eastern regions of the Mediterranean basin leading to extended drought periods (Majdalani et al., 2022).

Finally, drought durations (in days) for the low (237, 209), moderate (193, 157), and extreme (142, 43) soil desiccation thresholds were retrieved for the coastal and wettest mountainous zones, respectively. These estimates broadly align with the drought duration obtained in prior research, with a duration of 169 days as reported by Ruffault et al (2013), 155 days as reported by Lempereur et al (2015) in Mediterranean France, and 165 days according to Zribi et al (2016) in Tunisia.

Based on this assessment of drought features captured by DFEAT over Lebanon, when compared to previous studies, we aim at demonstrating the efficiency of our approach. Differences between studies can be attributed to the fixed thresholds above/below which soil moisture is considered sufficient to determine the end of the dry season and duration, a major weakness in current drought feature characterization lacking of standard protocols, and that DFEAT aims at fulfilling.

4.2. DFEAT response to the aridity gradient

We could demonstrate in this assessment exercise that DFEAT can be successfully applied under three different contrasted soil moisture dynamics, namely MED, HMED, and DRY-MED, reflecting typical soil desiccation along the Mediterranean aridity gradient in Lebanon, but also representative of Mediterranean climate extremes. MYD events have been increasingly studied due to their distinct characteristics and enduring impacts (Parry et al., 2012; Tsakiris et al., 2010; Van Der Wiel et al., 2023; Xu et al., 2021).

We could illustrate with DFEAT that MED drought-type for the low and moderate level predominates across all the Lebanese territory (90 % of the hydrological years), except the two less-watered governorates of Baalbeck-Hermel and Akkar, which are dominated but DRY-MED drought-type with MYD events, offering a biogeographical representation of drought in the country. No HMED drought-type is observed for the low and moderate drought level, indicating that under seasonal drought, soil lost at least 50 % of its AWC all over the country. This holds true under Mediterranean conditions (wet winter and dry summers), and is well documented across the basin (Lempereur et al., 2015; Zribi et al., 2016). We could find HMED drought-types for the extreme drought level (KBDI-150) covering exclusively two mountainous regions Mount-Lebanon and Anti-Lebanon with annual rainfall amounts exceeding 1200 mm/year and between 600 and 800 mm/year (Shaban, 2020). The precipitation patterns (climatic factor) and elevation (affecting temperatures and decreasing PET) (topographic/orographic factors) over

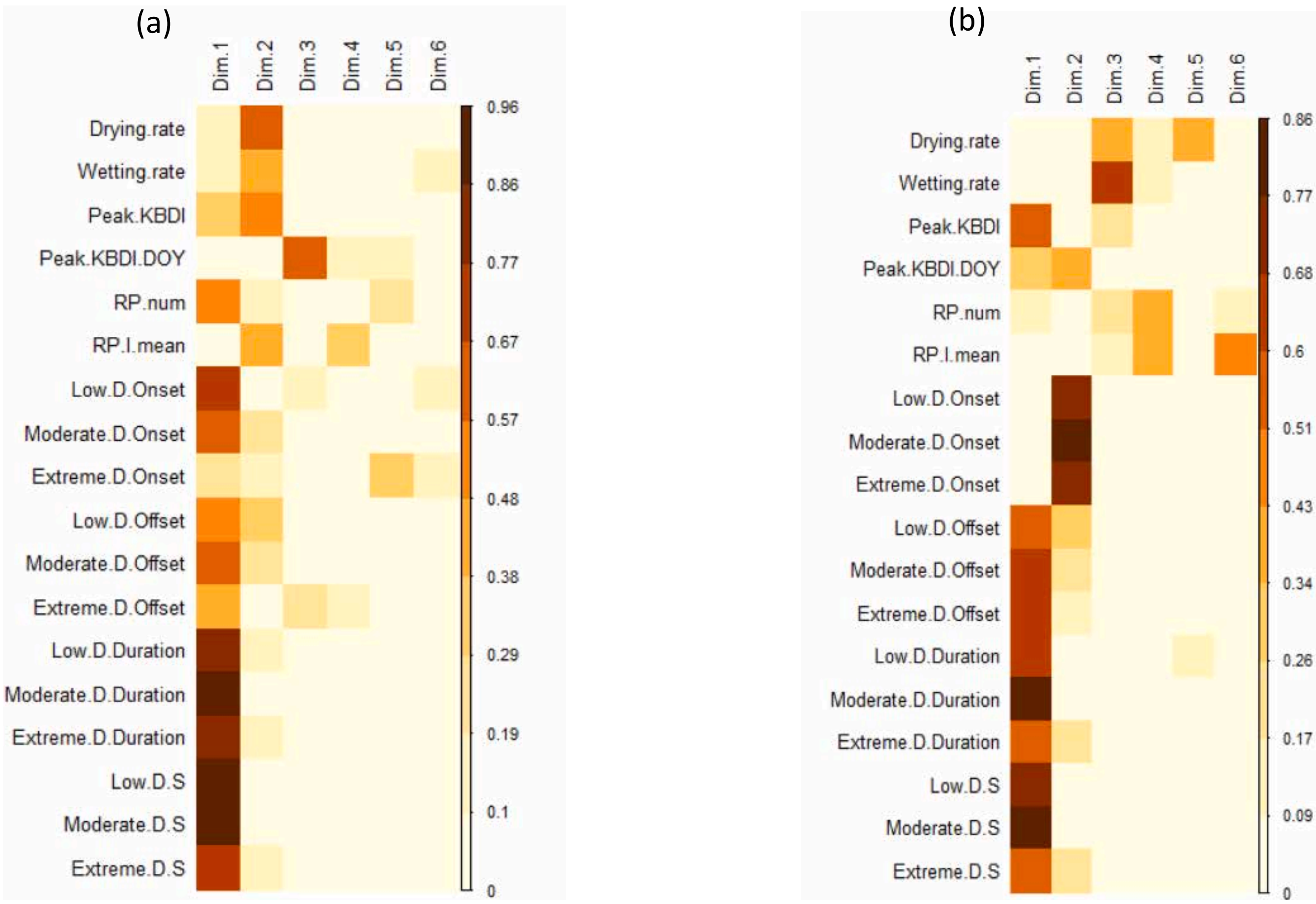

Fig. 10. a) Heat map illustrating the coefficient of squared correlation (cos2; square cosine, squared coordinates) of drought features on all dimensions (PCs) covering the entire country and b) for region experiencing only the MED and HMED drought-type. They represent the quality of representation for variables on a factor map. High cos2 values (Dark red and Marron squares) indicate a good representation of the drought features on the principal component (Dim.1, Dim.2, Dim.3, Dim.4, Dim.5, Dim.6). (For interpretation of the references to colour in this figure legend, the reader is referred to the web version of this article.)

both regions, could reasonably explain why extreme soil desiccation is not reached by the index.

We noted the absence of MYD for the extreme drought level all over the Lebanese territory (Fig. 7i), which suggests that there is always, at the very least, some seasonal precipitation (>50 mm/year), even in the most arid zones of Lebanon, capable of replenishing this depleted fraction from the soil. On the contrary, we detected MYD events when soils were not replenished (KBDI above the threshold 50 and 100) over subsequent hydrological years. In the two governorates of Akkar and Baalbeck-hermel, the duration of MYD events for the low (moderate) drought level could reach 23 (8) consecutive years without a full or nearly return to the soil field capacity (Fig. 8). Prolonged events of this nature have been observed in the region, with durations ranging between 3 years (Mathbout et al., 2021; Parry et al., 2012; Van Der Wiel et al., 2023) and 20 years (Wu et al., 2022a). However, the number of MYD events in Lebanon varies by microclimatic zones, getting less frequent over coastal, Southern, and wettest western mountainous zones. Yet, 1 to 2 MYD events could be captured by DFEAT in these regions (Fig. 7g-h), as in 1998–1999 and 2013–2014. These years were actually classified as the driest hydro-meteorological in the recent history of the country. As of 1999 and 2014, Lebanon was facing a summer drought after a record drought in 1998 and 2013 winters (Ghaleb et al., 2015; Kobrossi et al., 2021; Verner et al., 2018).

4.3. DFEAT applicability to other soil water balance models

In this first development and application of DFEAT, we assessed the characteristics of drought features over Lebanon, using the empirical daily soil water balance derived from KBDI. This index underwent testing in forestry and fire risk assessment (fire potential) at the global scale (Gannon and Steinberg, 2021; Liu et al., 2010; Snyder et al., 2006), and was tested under Mediterranean conditions in fire weather assessment studies conducted under Mediterranean conditions (Elhag and Boteva, 2021; Hamadeh et al., 2017). We acknowledge here that KBDI was also revisited for Mediterranean climate (Ganatsas et al., 2011), and that numerous other soil water balance models have been developed, from empirical equations (Andrade and Bugalho, 2023; Barbero et al., 2019; Nogueira et al., 2017) to more process-based models (Granier et al., 1999; Mouillot et al., 2001… among others), including preprocessed soil storage dataset as GLDAS (Li et al., 2019).

The Keetch-Byram Drought index assumes an arbitrary soil depth and a type of soil, with a water holding capacity of 203 mm (or 8 in.). However, the generalization is contingent on soil texture and depth, factors that can be discerned using available soil databases and maps (Ganatsas et al., 2011).

DFEAT framework could be applied to any other soil water balance model, whose impact on drought features should be further tested. We initiated a sensitivity analysis on temperatures locally varying in Mountainous areas leading to uncertainties of 2 to 22 % in most features, but additional sensitivity analysis related to PET equations (Berg and Sheffield, 2018; Ogunrinde et al., 2020; Tomas-Burguera et al., 2020), climate inputs (Hoffmann et al., 2020), or standardization method (Laimighofer and Laaha, 2022), and soil water balance models themselves should also be assessed.

4.4. Applications and limitations

While our study has successfully generated key drought features over hydrological years, it is important to acknowledge certain limitations that may impact the interpretation and generalization of the results when applied in agro-ecological studies (Espinosa et al., 2019; Gao et al., 2018). We have identified high correlations among most of the extracted drought features, including duration, severity, offset, and peak KBDI day of the year, a well-established phenomenon in drought feature assessments (McKee et al., 1993; Ruffault et al., 2013; Vicente-Serrano et al., 2010). Also, drought duration and severity can be regarded as the primary drought characteristics directly dependent on the onset and offset DOY determination (Deo et al., 2017). However, drought onset and offset are not exclusively correlated with each other, and appear to function somewhat independently.

This demonstrates that most of our drought features are not independent, but instead, are interconnected and may influence each other, which poses a challenge for interpreting their impacts (i.e., individual contribution of each feature) and explaining agro-environmental information (i.e., crop yields, tree radial growth, burned areas, tree mortality, plant phenology) when used together in statistical models (e.g., regression models). Accordingly, we suggest to process a multivariate analysis for the 19 drought features as an essential step for a more synthetic representation of drought in a given region, a common strategy used in community ecology where species are described by their interrelated traits and optimized reduced dimensionality has been proposed (Laughlin, 2014; Mouillot et al., 2021). This will lead to retain only the most representative and uncorrelated dimensions of drought, which will be more practically useful in agro-ecological applications (Espinosa et al., 2019; Huang et al., 2022; Santos et al., 2010; Vicente-Serrano et al., 2012).

As a first assessment, we could provide a reliable representation of drought features under contrasted soil drought dynamics (MED, HMED, DRY-MED drought-type) across the Mediterranean-type Lebanese aridity gradient, with one wet and one dry season per hydrological year. Further assessments should be launched to test for its applicability in diverse climatic zones, including regions with temperate climate, or those with a different seasonal distribution of annual rainfall, such as tropical region or those exhibiting a monsoon regime with two annual drought periods (Ferijal et al., 2021; Notaro et al., 2010). Also, drought impacts on agro- ecosystems have been shown to be enhanced when combined to thermal anomalies. Fire occurrence, for example, is constrained both by soil desiccation and heatwaves (Ruffault et al., 2020) likely to happen more frequently and concomitantly in a near future in Europe (Suarez-Gutierrez et al., 2023). As well, combined drought and heat during growing seasons might severely affect crop production (Guo et al., 2023). In turn, recent developments in hydrothermal indices combining drought and temperature anomalies have been developed (Li et al., 2021; Shan et al., 2023; Wu et al., 2022b). DFEAT V1.0 focuses in its initial development on soil water budget and will be tested across extended climate conditions and soil water models. Further hydrothermal indices will be proposed, as the mean or maximum temperatures reached between the drought onset and offset, peak KBDI DOY, or other critical periods based on end-users' requirements and feedbacks.

5. Conclusion

By leveraging water balance models and time series analytics, our proposed drought features assessment tool (DFEAT) fills the gap between daily soil water budgets models and annually-integrated drought indices as SPEI widely used for drought impact assessments. Based on a series of metrics that have been carefully selected following their potential impacts on agro-ecosystems, DFEAT has been able to extract a comprehensive set of features covering the entire drought development stages (onset, development/drying, persistence, peak, recovery/rewetting, and offset), through its application to an empirical daily simulated water balance (Mediterranean-calibrated version of KBDI). We could characterize contrasted regional drought pattern over the study area, with drought duration varying from 45 days in the Mountainous areas up to 23 years in the most arid zone and we could reduce drought characterization to 6 major features of duration/severity, onset timing, wetting rate, peak drought day, drying rate and rain pulse intensity as key components of drought. We could demonstrate its wide range of applicability for water-limited agro-ecosystems with a single dry period. We recommend the use of a standard protocol such as DFEAT to extract drought features from whatever daily soil water balance data, thus strengthening further synthesis and comparisons across independent studies.

Funding

The authors acknowledge the National Council for Scientific Research of Lebanon (CNRS-L), the French Embassy in Lebanon and Campus France for granting a doctoral fellowship to Georgie Elias.

CRediT authorship contribution statement

Georgie Elias: Writing – original draft, Visualization, Software, Methodology, Investigation, Formal analysis, Data curation, Conceptualization. **Ghaleb Faour:** Writing – review & editing, Supervision, Resources, Funding acquisition, Conceptualization. **Florent Mouillot:** Writing – review & editing, Visualization, Validation, Supervision, Resources, Project administration, Methodology, Funding acquisition, Conceptualization.

Declaration of competing interest

The authors declare that they have no known competing financial interests or personal relationships that could have appeared to influence the work reported in this paper.

Data availability

The data and model scripts presented in this study are available on request from the corresponding authors.

Acknowledgments

The authors express their gratitude to Alexandre Granier for his constructive recommendation to enhance the clarity and elaboration of the R code to run DFEAT. The authors also wish to express their gratitude to Victor Van der Meersch for his assistance in data curation and processing.

References

Ainuddin, N.A., Ampun, J., 2008. Temporal analysis of the keetch-byram drought index in Malaysia: implications for forest fire management. J. Appl. Sci. 8, 3991–3994.

Allam, M., Mhawej, M., Meng, Q., Faour, G., Abunnasr, Y., Fadel, A., Xinli, H., 2021. Monthly 10-m evapotranspiration rates retrieved by SEBALI with Sentinel-2 and MODIS LST data. Agric Water Manag 243, 106432. https://doi.org/10.1016/j.agwat.2020.106432.

Andrade, C., Bugalho, L., 2023. Multi-indices diagnosis of the conditions that led to the two 2017 major wildfires in Portugal. Fire 6, 56. https://doi.org/10.3390/fire6020056.

Barbero, R., Curt, T., Ganteaume, A., Maillé, E., Jappiot, M., Bellet, A., 2019. Simulating the effects of weather and climate on large wildfires in France. Nat. Hazards Earth Syst. Sci. 19, 441–454. https://doi.org/10.5194/nhess-19-441-2019.

Barbeta, A., Peñuelas, J., 2016. Sequence of plant responses to droughts of different timescales: lessons from holm oak (*Quercus ilex*) forests. Plant Ecolog. Divers. 9, 321–338. https://doi.org/10.1080/17550874.2016.1212288.

Barnard, R.L., Osborne, C.A., Firestone, M.K., 2015. Changing precipitation pattern alters soil microbial community response to wet-up under a Mediterranean-type climate. ISME J. 9, 946–957. https://doi.org/10.1038/ismej.2014.192.

Beck, P.S., Atzberger, C., Høgda, K.A., Johansen, B., Skidmore, A.K., 2006. Improved monitoring of vegetation dynamics at very high latitudes: A new method using

MODIS NDVI. Remote Sens. Environ. 100, 321–334. https://doi.org/10.1016/j.rse.2005.10.021.
Berg, A., Sheffield, J., 2018. Climate change and drought: the Soil moisture perspective. Curr. Clim. Change Rep. 4, 180–191. https://doi.org/10.1007/s40641-018-0095-0.
Beyene, T.K., Agarwal, A., Jain, M.K., Yadav, B.K., 2023. Investigation of the propagation of meteorological to hydrological drought and water required to recover from drought over Ethiopian basins. J. Water Clim. Chang. 14, 2988–3009. https://doi.org/10.2166/wcc.2023.024.
Bonsal, B.R., Wheaton, E.E., Meinert, A., Siemens, E., 2011. Characterizing the surface features of the 1999–2005 Canadian Prairie Drought in Relation to Previous Severe Twentieth Century Events. Atmos. Ocean 49, 320–338. https://doi.org/10.1080/07055900.2011.594024.
Brown, R.F., Sala, O.E., Sinsabaugh, R.L., Collins, S.L., 2022. Temporal effects of monsoon rainfall pulses on plant available nitrogen in a Chihuahuan Desert Grassland. JGR Biogeosciences 127, e2022JG006938. https://doi.org/10.1029/2022JG006938.
Brown, E.K., Wang, J., Feng, Y., 2021. US wildfire potential: A historical view and future projection using high-resolution climate data. Environ. Res. Lett. 16, 034060 https://doi.org/10.1088/1748-9326/aba868.
Collins, S.L., Belnap, J., Grimm, N.B., Rudgers, J.A., Dahm, C.N., D'Odorico, P., Litvak, M., Natvig, D.O., Peters, D.C., Pockman, W.T., Sinsabaugh, R.L., Wolf, B.O., 2014. A Multiscale, Hierarchical model of pulse dynamics in arid-land ecosystems. Annu. Rev. Ecol. Evol. Syst. 45, 397–419. https://doi.org/10.1146/annurev-ecolsys-120213-091650.
Core Team R, 2021. R: A Language and Environment for Statistical Computing [Computer Software]. R Foundation for Statistical Computing, Vienna, Austria.
Crane, W.J.B., 1982. Computing grassland and forest fire behaviour, relative humidity and drought index by pocket calculator. Aust. For. 45, 89–97. https://doi.org/10.1080/00049158.1982.10674339.
Deo, R.C., Byun, H.-R., Adamowski, J.F., Begum, K., 2017. Application of effective drought index for quantification of meteorological drought events: a case study in Australia. Theor. Appl. Climatol. 128, 359–379. https://doi.org/10.1007/s00704-015-1706-5.
Dimitrakopoulos, A.P., Bemmerzouk, A.M., 2003. Predicting live herbaceous moisture content from a seasonal drought index. Int. J. Biometeorol. 47, 73–79. https://doi.org/10.1007/s00484-002-0151-1.
Dodd, I.C., Puértolas, J., Huber, K., Pérez-Pérez, J.G., Wright, H.R., Blackwell, M.S., 2015. The importance of soil drying and re-wetting in crop phytohormonal and nutritional responses to deficit irrigation. J. Exp. Bot. 66, 2239–2252. https://doi.org/10.1093/jxb/eru532.
Edwards, D.C., McKee, T.B., 1997. Characteristics of 20th Century Drought in the United States at Multiple Time Scales.
Elhag, M., Boteva, S., 2021. The Canadian versus the National Forest Fire Danger Rating Systems tested in Mediterranean forests fire Crete, Greece. Environ.. Dev. Sustain. 23, 4973–4983. https://doi.org/10.1007/s10668-020-00799-7.
Elmore, A.J., Guinn, S.M., Minsley, B.J., Richardson, A.D., 2012. Landscape controls on the timing of spring, autumn, and growing season length in mid-Atlantic forests. Glob. Chang. Biol. 18, 656–674. https://doi.org/10.1111/j.1365-2486.2011.02521.x.
Espinosa, L.A., Portela, M.M., Pontes Filho, J.D., de Studart, T.M.C., Santos, J.F., Rodrigues, R., 2019. Jointly modeling drought characteristics with smoothed regionalized SPI series for a small island. Water 11, 2489. https://doi.org/10.3390/w11122489.
Ferijal, T., Batelaan, O., Shanafield, M., 2021. Rainy season drought severity trend analysis of the Indonesian maritime continent. Int. J. Climatol. 41 https://doi.org/10.1002/joc.6840.
Ferijal, T., Batelaan, O., Shanafield, M., Alfahmi, F., 2022. Determination of rainy season onset and cessation based on a flexible driest period. Theor. Appl. Climatol. 148, 91–104. https://doi.org/10.1007/s00704-021-03917-1.
Fung, K.F., Huang, Y.F., Koo, C.H., 2020. Assessing drought conditions through temporal pattern, spatial characteristic and operational accuracy indicated by SPI and SPEI: case analysis for Peninsular Malaysia. Nat. Hazards 103, 2071–2101. https://doi.org/10.1007/s11069-020-04072-y.
Ganatsas, P., Antonis, M., Marianthi, T., 2011. Development of an adapted empirical drought index to the Mediterranean conditions for use in forestry. Agric. For. Meteorol. 151, 241–250. https://doi.org/10.1016/j.agrformet.2010.10.011.
Gannon, C.S., Steinberg, N.C., 2021. A global assessment of wildfire potential under climate change utilizing Keetch-Byram drought index and land cover classifications. Environ. Res. Commun. 3, 035002 https://doi.org/10.1088/2515-7620/abd836.
Gao, S., Liu, R., Zhou, T., Fang, W., Yi, C., Lu, R., Zhao, X., Luo, H., 2018. Dynamic responses of tree-ring growth to multiple dimensions of drought. Glob. Chang. Biol. 24, 5380–5390. https://doi.org/10.1111/gcb.14367.
Gatien, P., Arsenault, R., Martel, J.-L., St-Hilaire, A., 2023. Using the ERA5 and ERA5-Land reanalysis datasets for river water temperature modelling in a data-scarce region. Can. Water Resour. J./Revue Canadienne Des Ressources Hydriques 48, 93–110. https://doi.org/10.1080/07011784.2022.2113917.
Ghaleb, F., Mario, M., Sandra, A.N., 2015. Regional landsat-based drought monitoring from 1982 to 2014. Climate 3, 563–577. https://doi.org/10.3390/cli3030563.
Glantz, M., 2003. Climate Affairs. Island Press.
Gomis-Cebolla, J., Rattayova, V., Salazar-Galán, S., Francés, F., 2023. Evaluation of ERA5 and ERA5-Land reanalysis precipitation datasets over Spain (1951–2020). Atmos. Res. 284, 106606 https://doi.org/10.1016/j.atmosres.2023.106606.
González-Hidalgo, J.C., Vicente-Serrano, S.M., Peña-Angulo, D., Salinas, C., Tomas-Burguera, M., Beguería, S., 2018. High-resolution spatio-temporal analyses of drought episodes in the western Mediterranean basin (Spanish mainland, Iberian Peninsula). Acta Geophys. 66, 381–392. https://doi.org/10.1007/s11600-018-0138-x.
Granier, A., Bréda, N., Biron, P., Villette, S., 1999. A lumped water balance model to evaluate duration and intensity of drought constraints in forest stands. Ecol. Model. 116, 269–283. https://doi.org/10.1016/S0304-3800(98)00205-1.
Gu, L., Post, W.M., Baldocchi, D.D., Black, T.A., Suyker, A.E., Verma, S.B., Vesala, T., Wofsy, S.C., 2009. Characterizing the seasonal dynamics of plant community photosynthesis across a range of vegetation types. In: Noormets, A. (Ed.), Phenology of Ecosystem Processes. Springer, New York, New York, NY, pp. 35–58. https://doi.org/10.1007/978-1-4419-0026-5_2.
Guo, Y., Zhang, J., Li, K., Aru, H., Feng, Z., Liu, X., Tong, Z., 2023. Quantifying hazard of drought and heat compound extreme events during maize (Zea mays L.) growing season using Magnitude Index and Copula. Weather Clim. Extremes 40, 100566. https://doi.org/10.1016/j.wace.2023.100566.
Gutiérrez, J.M., Ranasinghe, R., Ruane, A.C., Vautard, R., 2021. IPCC. Annex VI: Climatic impact-driver and extreme indices. Climate Change 2021: the Physical Science Basis. Contribution of Working Group I to the Sixth Assessment Report of the Intergovernmental Panel on Climate Change 2205–2214.
Hamadeh, N., Daya, B., Hilal, A., Chauvet, P., 2015. An analytical review on the most widely used meteorological models in forest fire prediction. In: 2015 Third International Conference on Technological Advances in Electrical, Electronics and Computer Engineering (TAEECE). IEEE, pp. 239–244. https://doi.org/10.1109/TAEECE.2015.7113633.
Hamadeh, N., Karouni, A., Daya, B., Chauvet, P., 2017. Using correlative data analysis to develop weather index that estimates the risk of forest fires in Lebanon & Mediterranean: Assessment versus prevalent meteorological indices. Case Stud. Fire Saf. 7, 8–22. https://doi.org/10.1016/j.csfs.2016.12.001.
Han, J., Singh, V.P., 2023. A review of widely used drought indices and the challenges of drought assessment under climate change. Environ. Monit. Assess. 195, 1438 https://doi.org/10.1007/s10661-023-12062-3.
Han, J., Zhang, J., Yang, S., Seka, A.M., 2023. Improved understanding of flash drought from a comparative analysis of drought with different intensification rates. Remote Sens. 15, 2049 https://doi.org/10.3390/rs15082049.
Häusler, M., Nunes, J.P., Silva, J.M., Keizer, J.J., Warneke, T., Pereira, J.M., 2019. A promising new approach to estimate drought indices for fire danger assessment using remotely sensed data. Agric. For. Meteorol. 274, 195–209. https://doi.org/10.1016/j.agrformet.2019.04.015.
Hoffmann, D., Gallant, A.J.E., Arblaster, J.M., 2020. Uncertainties in drought from index and data selection. JGR Atmos. 125, e2019JD031946 https://doi.org/10.1029/2019JD031946.
Huang, Y., Liu, B., Zhao, H., Yang, X., 2022. Spatial and temporal variation of droughts in the Mongolian Plateau during 1959–2018 based on the gridded self-calibrating Palmer Drought Severity Index. Water 14, 230. https://doi.org/10.3390/w14020230.
Hunt, E.D., Hubbard, K.G., Wilhite, D.A., Arkebauer, T.J., Dutcher, A.L., 2009. The development and evaluation of a soil moisture index. Int. J. Climatol. 29, 747–759. https://doi.org/10.1002/joc.1749.
Iglesias, V., Travis, W.R., Balch, J.K., 2022. Recent droughts in the United States are among the fastest-developing of the last seven decades. Weather Clim. Extremes 37, 100491. https://doi.org/10.1016/j.wace.2022.100491.
Jomaa, I., Abi Saab, M.T., Skaf, S., El Haj, N., Massaad, R., 2019. Variability in spatial distribution of precipitation overall rugged topography of Lebanon, using TRMM images. Atmos. Clim. Sci. 9, 369–380. https://doi.org/10.4236/acs.2019.93026.
Jönsson, P., Eklundh, L., 2004. TIMESAT—a program for analyzing time-series of satellite sensor data. Comput. Geosci. 30, 833–845. https://doi.org/10.1016/j.cageo.2004.05.006.
Karouni, A., Daya, B., Bahlak, S., 2013. A comparative study to find the most applicable fire weather index for Lebanon allowing to predict a forest fire. J. Commun. Comput. 11, 1403–1409.
Kassambara, A., 2016. Factoextra: extract and visualize the results of multivariate data analyses. R Package Version 1.
Keetch, J.J., Byram, G.M., 1968. A drought index for forest fire control. US Department of Agriculture, Forest Service, Southeastern Forest Experiment.
Kim, D.-W., Byun, H.-R., Choi, K.-S., Oh, S.-B., 2011. A spatiotemporal analysis of historical droughts in Korea. J. Appl. Meteorol. Climatol. 50, 1895–1912. https://doi.org/10.1175/2011JAMC2664.1.
Kobrossi, J., Karam, F., Mitri, G., 2021. Rain pattern analysis using the Standardized Precipitation Index for long-term drought characterization in Lebanon. Arab. J. Geosci. 14, 1–17. https://doi.org/10.1007/s12517-020-06387-3.
Kong, D., Zhang, Y., Wang, D., Chen, J., Gu, X., 2020. Photoperiod explains the asynchronization between vegetation carbon phenology and vegetation greenness phenology. JGR Biogeosci. 125, e2020JG005636 https://doi.org/10.1029/2020JG005636.
Kong, D., McVicar, T.R., Xiao, M., Zhang, Y., Peña-Arancibia, J.L., Filippa, G., Xie, Y., Gu, X., 2022. *phenofit*: An R package for extracting vegetation phenology from time series remote sensing. Methods Ecol. Evol. 13, 1508–1527. https://doi.org/10.1111/2041-210X.13870.
Laimighofer, J., Laaha, G., 2022. How standard are standardized drought indices? Uncertainty components for the SPI & SPEI case. J. Hydrol. 613, 128385 https://doi.org/10.1016/j.jhydrol.2022.128385.
Laughlin, D.C., 2014. The intrinsic dimensionality of plant traits and its relevance to community assembly. J. Ecol. 102, 186–193. https://doi.org/10.1111/1365-2745.12187.
Lê, S., Josse, J., Husson, F., 2008. FactoMineR: an R package for multivariate analysis. J. Stat. Softw. 25, 1–18. https://doi.org/10.18637/jss.v025.i01.

Lee, H., Calvin, K., Dasgupta, D., Krinner, G., Mukherji, A., Thorne, P., Trisos, C., Romero, J., Aldunce, P., Barrett, K., 2023. Climate change 2023: synthesis report. Contribution of Working Groups I, II and III to the Sixth Assessment Report of the Intergovernmental Panel on Climate Change. https://doi.org/10.59327/IPCC/AR6-9789291691647.

Lempereur, M., Martin-StPaul, N.K., Damesin, C., Joffre, R., Ourcival, J., Rocheteau, A., Rambal, S., 2015. Growth duration is a better predictor of stem increment than carbon supply in a Mediterranean oak forest: implications for assessing forest productivity under climate change. New Phytol. 207, 579–590. https://doi.org/10.1111/nph.13400.

Lempereur, M., Limousin, J., Guibal, F., Ourcival, J., Rambal, S., Ruffault, J., Mouillot, F., 2017. Recent climate hiatus revealed dual control by temperature and drought on the stem growth of Mediterranean *Quercus ilex*. Glob. Chang. Biol. 23, 42–55. https://doi.org/10.1111/gcb.13495.

Li, B., Rodell, M., Sheffield, J., Wood, E., Sutanudjaja, E., 2019. Long-term, non-anthropogenic groundwater storage changes simulated by three global-scale hydrological models. Sci. Rep. 9, 10746. https://doi.org/10.1038/s41598-019-47219-z.

Li, J., Wang, Z., Wu, X., Zscheischler, J., Guo, S., Chen, X., 2021. A standardized index for assessing sub-monthly compound dry and hot conditions with application in China. Hydrol. Earth Syst. Sci. 25, 1587–1601. https://doi.org/10.5194/hess-2020-383.

Lisonbee, J., Woloszyn, M., Skumanich, M., 2022. Making sense of flash drought: Definitions, indicators, and where we go from here. J. Appl. Serv. Climatol. https://doi.org/10.46275/JOASC.2021.02.001.

Liu, B., Liang, M., Huang, Z., Tan, X., 2021. Duration–severity–area characteristics of drought events in eastern China determined using a three-dimensional clustering method. Int. J. Climatol. 41 https://doi.org/10.1002/joc.6904.

Liu, Y., Stanturf, J., Goodrick, S., 2010. Trends in global wildfire potential in a changing climate. For. Ecol. Manage. 259, 685–697. https://doi.org/10.1016/j.foreco.2009.09.002.

Liu, Y., Zhu, Y., Zhang, L., Ren, L., Yuan, F., Yang, X., Jiang, S., 2020. Flash droughts characterization over China: From a perspective of the rapid intensification rate. Sci. Total Environ. 704, 135373 https://doi.org/10.1016/j.scitotenv.2019.135373.

Loik, M.E., Breshears, D.D., Lauenroth, W.K., Belnap, J., 2004. A multi-scale perspective of water pulses in dryland ecosystems: climatology and ecohydrology of the western USA. Oecologia 141, 269–281. https://doi.org/10.1007/s00442-004-1570-y.

López-Ballesteros, A., Serrano-Ortiz, P., Sánchez-Cañete, E.P., Oyonarte, C., Kowalski, A. S., Pérez-Priego, Ó., Domingo, F., 2016. Enhancement of the net CO_2 release of a semiarid grassland in SE Spain by rain pulses. JGR Biogeosci. 121, 52–66. https://doi.org/10.1002/2015JG003091.

Lu, E., 2009. Determining the start, duration, and strength of flood and drought with daily precipitation: Rationale. Geophys. Res. Lett. 36, 2009GL038817 https://doi.org/10.1029/2009GL038817.

Lu, E., Cai, W., Jiang, Z., Zhang, Q., Zhang, C., Higgins, R.W., Halpert, M.S., 2014. The day-to-day monitoring of the 2011 severe drought in China. Clim. Dyn. 43, 1–9. https://doi.org/10.1007/s00382-013-1987-2.

Majdalani, G., Koutsias, N., Faour, G., Adjizian-Gerard, J., Mouillot, F., 2022. Fire Regime Analysis in Lebanon (2001–2020): Combining remote sensing data in a scarcely documented area. Fire 5, 141. https://doi.org/10.3390/fire5050141.

Manzoni, S., Chakrawal, A., Fischer, T., Schimel, J.P., Porporato, A., Vico, G., 2020. Rainfall intensification increases the contribution of rewetting pulses to soil heterotrophic respiration. Biogeosciences 17, 4007–4023. https://doi.org/10.5194/bg-17-4007-2020.

Mathbout, S., Lopez-Bustins, J.A., Royé, D., Martin-Vide, J., 2021. Mediterranean-scale drought: Regional datasets for exceptional meteorological drought events during 1975–2019. Atmosphere 12, 941. https://doi.org/10.3390/atmos12080941.

McKee, T.B., Doesken, N.J., Kleist, J., 1993. The relationship of drought frequency and duration to time scales. In: Proceedings of the 8th Conference on Applied Climatology. California, pp. 179–183.

Mitri, G., Jazi, M., McWethy, D., 2014b. Assessing Lebanon's wildfire potential in association with current and future climatic conditions. In: Proc. of the Large Wildland Fires Conf. pp. 301–304.

Mitri, G., Jazi, M., McWethy, D., 2014a. Investigating temporal and spatial variability of wildfire potential with the use of objectbased image analysis of downscaled global climate models. South-Eastern Eur. J. Earth Observ. Geomat. 3, 251–254.

Mouillot, D., Loiseau, N., Grenié, M., Algar, A.C., Allegra, M., Cadotte, M.W., Casajus, N., Denelle, P., Guéguen, M., Maire, A., Maitner, B., McGill, B.J., McLean, M., Mouquet, N., Munoz, F., Thuiller, W., Villéger, S., Violle, C., Auber, A., 2021. The dimensionality and structure of species trait spaces. Ecol. Lett. 24, 1988–2009. https://doi.org/10.1111/ele.13778.

Mouillot, F., Rambal, S., Lavorel, S., 2001. A generic process-based SImulator for meditERRanean landscApes (SIERRA): design and validation exercises. For. Ecol. Manage. 147, 75–97. https://doi.org/10.1016/S0378-1127(00)00432-1.

Muñoz-Sabater, J., Dutra, E., Agustí-Panareda, A., Albergel, C., Arduini, G., Balsamo, G., Boussetta, S., Choulga, M., Harrigan, S., Hersbach, H., 2021. ERA5-Land: A state-of-the-art global reanalysis dataset for land applications. Earth Syst. Sci. Data 13, 4349–4383. https://doi.org/10.5194/essd-13-4349-2021.

Nogueira, J.M., Rambal, S., Barbosa, J.P.R., Mouillot, F., 2017. Spatial pattern of the seasonal drought/burned area relationship across Brazilian biomes: Sensitivity to drought metrics and global remote-sensing fire products. Climate 5, 42. https://doi.org/10.3390/cli5020042.

Notaro, M., Liu, Z., Gallimore, R.G., Williams, J.W., Gutzler, D.S., Collins, S., 2010. Complex seasonal cycle of ecohydrology in the Southwest United States, 2010JG001382 J. Geophys. Res. 115. https://doi.org/10.1029/2010JG001382.

Novitasari, N., Sujono, J., Harto, S., Maas, A., Jayadi, R., 2019. Drought index for peatland wildfire management in central Kalimantan, Indonesia during El Niño phenomenon. J. Disaster Res. 14, 939–948. https://doi.org/10.20965/jdr.2019.p0939.

Ogunrinde, A.T., Olasehinde, D.A., Olotu, Y., 2020. Assessing the sensitivity of standardized precipitation evapotranspiration index to three potential evapotranspiration models in Nigeria. Sci. Afr. 8, e00431 https://doi.org/10.1016/j.sciaf.2020.e00431.

Otkin, J.A., Svoboda, M., Hunt, E.D., Ford, T.W., Anderson, M.C., Hain, C., Basara, J.B., 2018. Flash droughts: A review and assessment of the challenges imposed by rapid-onset droughts in the United States. Bull. Am. Meteorol. Soc. 99, 911–919. https://doi.org/10.1175/BAMS-D-17-0149.1.

Oukaddour, K., Le Page, M., Fakir, Y., 2024. Toward a redefinition of agricultural drought periods. A case study in a Mediterranean Semi-arid region. Remote Sens 16, 83. https://doi.org/10.3390/rs16010083.

Pachauri, R.K., Allen, M.R., Barros, V.R., Broome, J., Cramer, W., Christ, R., Church, J.A., Clarke, L., Dahe, Q., Dasgupta, P., 2014. Climate change 2014: synthesis report. Contribution of Working Groups I, II and III to the fifth assessment report of the Intergovernmental Panel on Climate Change. IPCC.

Parry, S., Hannaford, J., Lloyd-Hughes, B., Prudhomme, C., 2012. Multi-year droughts in Europe: analysis of development and causes. Hydrol. Res. 43, 689–706. https://doi.org/10.2166/nh.2012.024.

Pellizzaro, G., Cesaraccio, C., Duce, P., Ventura, A., Zara, P., 2007. Relationships between seasonal patterns of live fuel moisture and meteorological drought indices for Mediterranean shrubland species. Int. J. Wildland Fire 16, 232–241. https://doi.org/10.1071/WF06081.

Pockman, W.T., Small, E.E., 2010. The influence of spatial patterns of soil moisture on the grass and shrub responses to a summer rainstorm in a Chihuahuan Desert Ecotone. Ecosystems 13, 511–525. https://doi.org/10.1007/s10021-010-9337-2.

Qing, Y., Wang, S., Yang, Z.-L., Gentine, P., Zhang, B., Alexander, J., 2023. Accelerated soil drying linked to increasing evaporative demand in wet regions. npj Clim. Atmos. Sci. 6, 205. https://doi.org/10.1038/s41612-023-00531-y.

Rahmat, S.N., Jayasuriya, N., Bhuiyan, M., 2015. Assessing droughts using meteorological drought indices in Victoria, Australia. Hydrol. Res. 46, 463–476. https://doi.org/10.2166/nh.2014.105.

Ruffault, J., Martin-StPaul, N.K., Rambal, S., Mouillot, F., 2013. Differential regional responses in drought length, intensity and timing to recent climate changes in a Mediterranean forested ecosystem. Clim. Change 117, 103–117. https://doi.org/10.1007/s10584-012-0559-5.

Ruffault, J., Martin-StPaul, N., Pimont, F., Dupuy, J.-L., 2018. How well do meteorological drought indices predict live fuel moisture content (LFMC)? An assessment for wildfire research and operations in Mediterranean ecosystems. Agric. For. Meteorol. 262, 391–401. https://doi.org/10.1016/j.agrformet.2018.07.031.

Ruffault, J., Curt, T., Moron, V., Trigo, R.M., Mouillot, F., Koutsias, N., Pimont, F., Martin-StPaul, N., Barbero, R., Dupuy, J.-L., 2020. Increased likelihood of heat-induced large wildfires in the Mediterranean Basin. Sci. Rep. 10, 13790. https://doi.org/10.1038/s41598-020-70069-z.

Salehnia, N., Zare, H., Kolsoumi, S., Bannayan, M., 2018. Predictive value of Keetch-Byram Drought Index for cereal yields in a semi-arid environment. Theor. Appl. Climatol. 134, 1005–1014. https://doi.org/10.1007/s00704-017-2315-2.

Salloum, L., Mitri, G., 2014. Assessment of the temporal pattern of fire activity and weather variability in Lebanon. Int. J. Wildland Fire 23, 503–509. https://doi.org/10.1071/WF12101.

Santos, J.F., Pulido-Calvo, I., Portela, M.M., 2010. Spatial and temporal variability of droughts in Portugal. Water Resour. Res. 46, 2009WR008071 https://doi.org/10.1029/2009WR008071.

Shaban, A., 2020. Water Resources of Lebanon World Water Resources. Springer International Publishing, Cham doi: 10.1007/978-3-030-48717-1.

Shaban, A., Awad, M., Ghandour, A.J., Telesca, L., 2019. A 32-year aridity analysis: a tool for better understanding on water resources management in Lebanon. Acta Geophys. 67, 1179–1189. https://doi.org/10.1007/s11600-019-00300-7.

Shan, B., Verhoest, N.E., De Baets, B., 2023. Identification of compound drought and heatwave events on a daily scale and across four seasons. Egusphere 2023, 1–21. https://doi.org/10.5194/egusphere-2023-147.

Sharma, S., 1995. Applied Multivariate Techniques. John Wiley & Sons Inc.

Shrestha, A.B., Bajracharya, S.R., Sharma, A.R., Duo, C., Kulkarni, A., 2017. Observed trends and changes in daily temperature and precipitation extremes over the Koshi river basin 1975–2010. Int. J. Climatol. 37, 1066–1083. https://doi.org/10.1002/joc.4761.

Singh, N.K., Emanuel, R.E., McGlynn, B.L., Miniat, C.F., 2021. Soil moisture responses to rainfall: implications for runoff generation. Water Resour. Res. 57, e2020WR028827 https://doi.org/10.1029/2020WR028827.

Snyder, R.L., Spano, D., Duce, P., Baldocchi, D., Xu, L., 2006. A fuel dryness index for grassland fire-danger assessment. Agric. For. Meteorol. 139, 1–11. https://doi.org/10.1016/j.agrformet.2006.05.006.

Suarez-Gutierrez, L., Müller, W., Marotzke, J., 2023. Extreme heat and drought typical of an end-of-century climate could occur over Europe soon and repeatedly. Commun. Earth. Environ. 4, 415. https://doi.org/10.1038/s43247-023-01075-y.

Tomas-Burguera, M., Vicente-Serrano, S.M., Peña-Angulo, D., Domínguez-Castro, F., Noguera, I., El Kenawy, A., 2020. Global characterization of the varying responses of the standardized precipitation evapotranspiration index to atmospheric evaporative demand. JGR Atmos. 125, e2020JD033017 https://doi.org/10.1029/2020JD033017.

Tramblay, Y., Koutroulis, A., Samaniego, L., Vicente-Serrano, S.M., Volaire, F., Boone, A., Le Page, M., Llasat, M.C., Albergel, C., Burak, S., Cailleret, M., Kalin, K.C., Davi, H., Dupuy, J.-L., Greve, P., Grillakis, M., Hanich, L., Jarlan, L., Martin St-Paul, N., Martinez-Vilalta, J., Mouillot, F., Pulido-Velazquez, D., Quintana-Segui, P., Renard, D., Turco, M., Turkes, M., Trigo, R., Vidal, J.-P., Vilagrosa, A., Zribi, M., Polcher, J.

2020. Challenges for drought assessment in the Mediterranean region under future climate scenarios. Earth Sci. Rev. 210, 103348. https://doi.org/10.1016/j.earscirev.2020.103348.
Tsakiris, G., Loukas, A., Pangalou, D., Vangelis, H., Tigkas, D., Rossi, G., Cancelliere, A., 2007. Drought characterization. Drought Management Guidelines Technical Annex 58, 85–102.
Tsakiris, G., Vangelis, H., Tigkas, D., 2010. Assessing water system vulnerability to multi-year droughts. Eur. Water 29, 21–29.
Van Der Wiel, K., Batelaan, T.J., Wanders, N., 2023. Large increases of multi-year droughts in north-western Europe in a warmer climate. Clim. Dyn. 60, 1781–1800. https://doi.org/10.1007/s00382-022-06373-3.
Vargas, R., Collins, S.L., Thomey, M.L., Johnson, J.E., Brown, R.F., Natvig, D.O., Friggens, M.T., 2012. Precipitation variability and fire influence the temporal dynamics of soil CO_2 efflux in an arid grassland. Glob. Chang. Biol. 18, 1401–1411. https://doi.org/10.1111/j.1365-2486.2011.02628.x.
Varol, T., Ertuğrul, M., 2016. Analysis of the forest fires in the Antalya region of Turkey using the Keetch-Byram drought index. J. For. Res. 27, 811–819. https://doi.org/10.1007/s11676-016-0235-0.
Verner, D., Ashwill, M., Christensen, J., Mcdonnell, R., Redwood, J., Jomaa, I., Saade, M., Massad, R., Chehade, A., Bitar, A., 2018. Droughts and Agriculture in Lebanon: Causes, Consequences, and Risk Management. World Bank.
Vicente-Serrano, S.M., Beguería, S., López-Moreno, J.I., 2010. A multiscalar drought index sensitive to global warming: the standardized precipitation evapotranspiration index. J. Clim. 23, 1696–1718. https://doi.org/10.1175/2009JCLI2909.1.
Vicente-Serrano, S.M., Beguería, S., Lorenzo-Lacruz, J., Camarero, J.J., López-Moreno, J.I., Azorin-Molina, C., Revuelto, J., Morán-Tejeda, E., Sanchez-Lorenzo, A., 2012. Performance of drought indices for ecological, agricultural, and hydrological applications. Earth Interact. 16, 1–27. https://doi.org/10.1175/2012EI000434.1.
Vicente-Serrano, S.M., Camarero, J.J., Azorin-Molina, C., 2014. Diverse responses of forest growth to drought time-scales in the Northern Hemisphere. Glob. Ecol. Biogeogr. 23, 1019–1030. https://doi.org/10.1111/geb.12183.
Vogel, J., Paton, E., Aich, V., Bronstert, A., 2021. Increasing compound warm spells and droughts in the Mediterranean Basin. Weather Clim. Extremes 32, 100312. https://doi.org/10.1016/j.wace.2021.100312.
Wang, Q., Zeng, J., Qi, J., Zhang, X., Zeng, Y., Shui, W., Xu, Z., Zhang, R., Wu, X., Cong, J., 2021. A multi-scale daily SPEI dataset for drought characterization at observation stations over mainland China from 1961 to 2018. Earth Syst. Sci. Data 13 (331–341), 2021. https://doi.org/10.5194/essd-13-331-2021.
Wilhite, D.A., Glantz, M.H., 1985. Understanding: the drought phenomenon: the role of definitions. Water Int. 10, 111–120. https://doi.org/10.1080/02508068508686328.
Wu, G., Chen, J., Kim, J.-S., Gu, L., Lee, J.-H., Zhang, L., 2022a. Impacts of climate change on global meteorological multi-year droughts using the last millennium simulation as a baseline. J. Hydrol. 610, 127937 https://doi.org/10.1016/j.jhydrol.2022.127937.
Wu, T., Li, B., Lian, L., Zhu, Y., Chen, Y., 2022b. Assessment of the combined risk of drought and high-temperature heat wave events in the North China plain during summer. Remote Sens. (Basel) 14, 4588. https://doi.org/10.3390/rs14184588.
Xu, C., Ke, Y., Zhou, W., Luo, W., Ma, W., Song, L., Smith, M.D., Hoover, D.L., Wilcox, K.R., Fu, W., 2021. Resistance and resilience of a semi-arid grassland to multi-year extreme drought. Ecol. Ind. 131, 108139 https://doi.org/10.1016/j.ecolind.2021.108139.
Yevjevich, V.M., 1967. Objective Approach to Definitions and Investigations of Continental Hydrologic Droughts. PhD Thesis. Colorado State University. Libraries.
Yoo, J., Kim, J., Kwon, H.-H., Kim, T.-W., 2022. A new drought monitoring approach using three-dimensional drought properties based on a dynamic drought detection technique algorithm. J. Hydrol.: Reg. Stud. 44, 101270 https://doi.org/10.1016/j.ejrh.2022.101270.
Zargar, A., Sadiq, R., Naser, B., Khan, F.I., 2011. A review of drought indices. Environ. Rev. 19, 333–349. https://doi.org/10.1139/a11-013.
Zhang, X., Friedl, M.A., Schaaf, C.B., Strahler, A.H., Hodges, J.C., Gao, F., Reed, B.C., Huete, A., 2003. Monitoring vegetation phenology using MODIS. Remote Sens. Environ. 84, 471–475. https://doi.org/10.1016/S0034-4257(02)00135-9.
Zhang, X., Duan, Y., Duan, J., Jian, D., Ma, Z., 2022. A daily drought index based on evapotranspiration and its application in regional drought analyses. Sci. China Earth Sci. 65, 317–336. https://doi.org/10.1007/s11430-021-9822-y.
Zhang, L., Wang, Y., Sun, Z., 2023. Soil water depletion patterns in rainfed apple orchards and wheat fields. PeerJ 11, e15098. https://doi.org/10.7717/peerj.15098.
Zhang, X., Yang, F., 2004. RClimDex (1.0) User Manual. Climate Research Branch Environment Canada 22, 13–14.
Zhao, F., Liu, Y., 2021. Important meteorological predictors for long-range wildfires in China. For. Ecol. Manage. 499, 119638 https://doi.org/10.1016/j.foreco.2021.119638.
Zribi, L., Mouillot, F., Guibal, F., Rejeb, S., Rejeb, M.N., Gharbi, F., 2016. Deep soil conditions make Mediterranean cork oak stem growth vulnerable to autumnal rainfall decline in Tunisia. Forests 7, 245. https://doi.org/10.3390/f7100245.